University of Sheffield

University of Sheffield

A thesis submitted in partial fulfilment
for the degree of Doctor of Philosophy

in the Faculty of Science
Department of Physics and Astronomy

Mechanical modelling of phagocytosis and constricted migration.

Author: Mehdi AIT YAHIA

July, 2024.

Abstract

In this work we take a theoretical modelling approach to cell mechanics. The mechanical properties we focus on are the elastic reshaping and force generation by the cell. From the membrane lipid bilayer to the nucleus and cortex we explore how they can play a role in affecting two important processes for cells: endocytosis in its diverse forms and constriction crossing. The first process we consider is the take up of a solid particle and consider the influence of curvature and size on the ability of completing engulfment to discuss the optimal configuration as suggested in experiments and simulation. Then we focus on the time evolution of engulfment starting with an already formed cup we propose a model based on fluid mechanics to explain the time evolution observed. Finally we study the nucleus in the context of constriction crossing. We consider its elasticity combined to the constriction size with static friction and how they end up determining the possibility of crossing or not. Moreover we build a model to get the probability of crossing with constriction size that can be compared to experimental observation for discussion.

Acknowledgements

First, I want to thank my supervisors Dr.Rhoda Hawkins and Dr.Simon Johnston for the support and advice on my work during the whole PhD from the beginning to the end. I also thank Chack, Matt and Tanju for their mental support and encouragement. I would also like to thank my family and friends for their continuous support before and during the PhD. I am thankful to Dr. Jaime Cañedo for the discussions on biology. I also thank Professor Clive Tadhunter for the advices as a mentor during the PhD.
I acknowledge EPSRC for funding.

Contents

Chapter 1

Introduction

1.1 Introduction

1.1.1 Key elements

To describe the diversity observed in nature the living systems are often classified in groups and subgroups called the phylogenic tree. This tree goes back to more primordial organisms. The living organisms have in common the cell as a fundamental element at the microscale storing the information and playing a first role in determining the phenotype of the organism. When looking at the microscopic scale we can observe the cell performing different tasks like processing the information stored in the DNA, replication or defending from pathogens that want to invade the organism. To move and deform in its environment the cell interacts with the environment. A macrophage for example requires movement in order to track a moving target like a bacteria or any pathogen. On the other hand the cell needs a signalling to be guided in the near environment. The signal through a spatial gradient directs the velocity vector to track a target. The cell operates with its environment through the interaction with chemicals triggering the cell. The barrier between the inside and the outside is a thin membrane layer with a thickness of few nanometres. The cell has a diameter of 15 μm [1] and composed of many elements in interaction and coupled. We introduce the key elements that we will meet in the following sections to have a better understanding of this biological machinery:

1. The plasma membrane is constituted of two layers of lipid molecules called the lipid bilayer (see fig.1). The bilayer is made of lipid molecules ordered and forming the building blocks of the membrane. Those molecules can be represented with a head and tail structure. The head is hydrophilic and tends to prefer interaction with water. On the other hand the tail of the molecule is hydrophobic. They tend to self organise in water with head oriented to the outside and tails to the inside of the bilayer. The thickness of the plasma membrane is estimated to be around $5nm$[1].

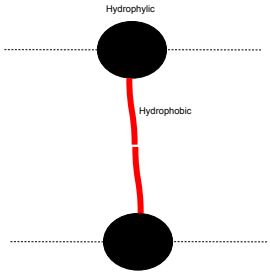

Figure 1.1: Two lipid molecules with hydrophobic tails pointing to each other and the hydrophylic heads facing water molecules. It creates a double layer of lipids commonly called the lipid bilayer.

2. The cytoplasm is the fluid present between the cell membrane and the nucleus. Its viscosity is estimated to be between 2 and 20 mPa.s [18] which is few times higher compared to water.

3. The nucleus is a few microns in diameters and delimited by the nuclear envelope and lamina. Inside the nucleus we find the DNA structured within the chromatin. Its stiffer than the cell membrane and cytoplasm.

4. The cytoskeleton (see fig.1.2) is the combination of three main components: Actin filaments, microtubules and intermediate filament. It generates the force needed for the cell to complete different processes maintaining and adapting cell shape to the situation, cell division or migration. It is the active part of the cell generating motion.

1.1.2 Introducing endocytosis

We distinguish two size dependent processes: phagocytosis for relatively large targets (usually $> 0.5\mu m$) and other endocytosis process. The main difference lies in the way the membrane reshapes to engulf the particle. Clathrin-mediated (a coating on the vesicle) endocytosis goes through a deformation of the membrane by binding with the target to the interior of the cell. Pinocytosis is a cell drinking process accompagnied by macromolecules for larger volumes we talk about macropinocytosis and will come back on this later in section 1.3.3. Phagocytosis is assumed to occur for sizes above $0.5\mu m$ but no theoretical rule exists on this value. Phagocytosis requires the formation of a phagocytic cup fuelled by the active forces of actin to be able to engulf the target. It requires the cell to move towards the bead with extensions called pseudopods working like cell extensions with the help of actin. The process may also require adhesion with a surface coating. From the observation of large deformation to engulf the bead we are required to understand how the membrane is structured in order to

have the best description to model it in theoretical and numerical work. Models for phagocytosis include usually the effect of adhesion between the target and the membrane to ensure the engulfment with the progression of the phagocytosis. Under the lipid bilayer membrane the cortex, made of actin, is supposed to generate enough force to complete the engulfment of the membrane around the target.

1.2 Introduction to cell structure

1.2.1 Lipid bilayer membrane

In order to complete phagocytosis the target must be encapsulated in a phagosome. Experimentally cells are able to take up targets with a size close to its own diameter. This obviously requires an extension of the initial surface of the plasma membrane and a significant reshaping of the cell. Despite the fact that the complete mechanism seems unresolved some hints may be given on the way the cell works to handle the situation. The membrane can curve out of its original curvature which requires energy that can come from Brownian motion and energy from the cell using ATP. The cortex with actin filaments is the active material under the membrane involved in phagocytosis and macropinocytosis for example. The lipid bilayer is stretchable to a maximum of few extra percents (reviewed in [30]). The membrane being wrinkled we can expect a contribution from this part leading to a "smoother" surface during high extensions. Passing a given threshold the force increases exponentially indicating perhaps that after using the maximum surface available to generate more surface the plasma may start to stretch and reduce the number of wrinkles to optimise the surface. Different from stretching, exocytosis can increase the total surface of a cell and plays the role of a membrane reservoir by expelling small vesicles from the cell and at the same time increasing the total surface by adding small patches when fusing with the membrane. The mechanical properties of the lipid bilayer depends on the lipid phase, for example the Young's modulus can go from 19.3 MPa in a liquid phase and 28.1 MPa in a gel phase [27].

1.2.2 Actin from monomers to filaments

Actin monomers are composed of 375 amino acids and have a molecular weight of 43 kDa [19]. Actin filaments, made of actin monomers, can represent up to 10% of the total number of proteins especially in skeletal muscle cells that generate more force. From the actin filaments we end up with a gel forming a network that has viscoelastic properties and at the same time is active with the polymerysation generating force and myosin, a motor protein generating force, for cortical tension. F-actin or actin filaments in the cytoskeleton are the result of the polymerisation (see fig.1.3) of monomers called G-actin into longer filaments with a persistence length l_p of $15\mu m$ and $6-8nm$ in diameter [19]. Actin polymerisation fuelled by ATP hydrolysis is regulated by actin-binding proteins.

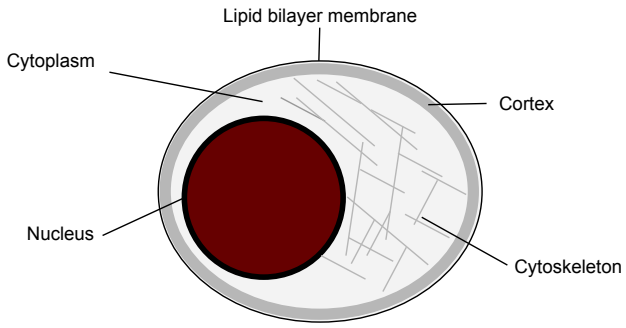

Figure 1.2: Diagram of the cell and its main elements defining the mechanical properties: elasticity and force generation.

Each protein group exhibits different properties, for example ADF/cofilin cutting filaments and profilin binding monomers [22]. Changing the length and density of filaments end up determining the gel phase on a macroscale with the viscoelastic properties of the assembly. Depending on the difference between the two rates k_+ for polymerisation rate and k_- corresponding to the depolymerisation rate, the actin filament can through treadmilling , when $k_+ = k_-$, appear to move by polymerising on one pole of the filament and depolymerising on the other pole without changing the total length of the filament. The persistence length is a way to describe the type of polymer by comparing it with the length of the polymer. If the persistence length l_p is very large compared to the total length of the polymer l we will expect a very constant shape of the polymer like a straight line. On the other hand the case where $l_p << l$ the polymer can be described as a disjointed chain or a random walk with a constant step size. Flexible and semi-flexible can be distinguish by the way they are described. A flexible polymer can be depicted as a random walk. On the other side a semi-flexible will be more rigid and the introduction of an elasticity can be more realistic.

The overall properties of the structure depends on the density and nature of actin filaments. We can distinguish different types of macromelucar polymers. The temperature and elasticity of a semi flexible polymer can be found in the formula of the persistence length

$$l_p = \frac{K}{k_b T} \tag{1.1}$$

with K the bending stiffness, k_b the Boltzmann constant and T the temperature in Kelvin.

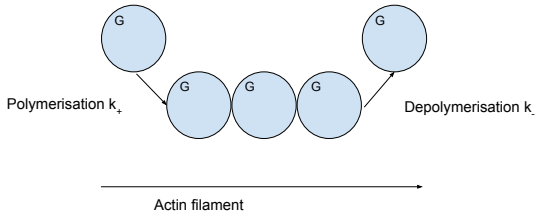

Figure 1.3: Representation of an actin filament with a schematic representation of the actin monomers G-Actin represented by the letter G. The rates k_+ and k_- on both ends represent the faster end (or barbed) and the slower end (or pointed) respectively.

1.2.3 Cytoskeleton

The cytoskeleton as the name may suggest corresponds to the essential "rigid" structure of the cell built like a network of the different actin filament structures giving it the capacity to withstand external forces. The cytoskeleton has as building blocks elements different filaments and proteins connected into a network giving rise to its mechanical properties like cell stiffness and viscous properties. The most commonly found in literature are actin filaments, microtubules and intermediate filaments. The cytoskeleton is fundamental for migration and defining cell shape. A fundamental structure in cell membrane reshaping is the cortex with a higher density of actin filaments compared to other regions of the cytoskeleton in the cell.

1.2.4 Cortex

Under the lipid bilayer membrane is the cortex (see fig.1.2). It is the regulator of the shape through force generation and its active properties. The thickness and density are subject to change for example the formation of blebs can momentarily increase the cortex thickness or even have an inhomogeneous thickness transversely (reviewed in [8]). From there we should keep in mind when interpreting results and consider a range of possible values or averages instead since that depending on the situation things can be very different as the cell has adaptation capacities. To describe the elasticity of the membrane we have to

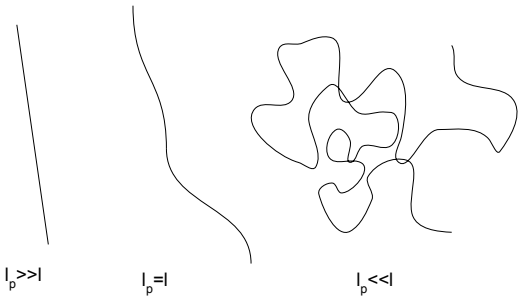

Figure 1.4: General description on how a polymer can be described depending on the bending stiffness K_B. We go from a straight line for $l_p >> l$ on the left to the other extreme on the right $l_p << l$.

define what we mean by membrane. In general it consists on the lipid bilayer with a thickness of few nanometres described in section 1.2.1. In addition to the lipid bilayer and its properties we have to consider the actomyosin cortex as a main element of the total new membrane lipid bilayer and cortex. In fact both are connected. The ezrin from the ERM group (Ezrin-Radixin-Moesin) [25] attaching the membrane to the cortex and playing a role in the blebs formation when the cortex is more detached from the plasma membrane.

The cortex structure is far more complex in terms of composition and geometrical structure than the lipid bilayer which makes it difficult to physically describe. Models like the one developed by Satcher and Dewey for example (reviwed in [22]) consider the mesh size being 100 nm and the cortex as a meshwork of connected rods forming a porous medium. This meshsize is also reviewed in [8] in more recent work. Despite the attempt to estimate Young's modulus to characterise the elasticity of the cortex it is still an active material that adapts to its environment and function that is why talking about a fixed value of the modulus may be misleading. Techniques like Atomic Force Microscopy where a cantilever is used to scan the cell surface and record the elastic response can be ambiguous to interpret since we don't know what is responding to the membrane lipid bilayer. The response can be from an active process and mimic a higher elasticity. The cortex has physical properties that we can list:

1. Viscoelasticity depending on the frequency or timescale. Considered as an elastic solid under 1 min and a viscous fluid otherwise[8]. An order of magnitude close to 10 kPa can be found in the literature regarding cortex stiffness [11] [21].

2. Cortex tension. Resulting from the actomyosin network with the actin filament attached by crosslinkers.

3. Frictional forces from the interaction with the membrane.

4. Stiffness especially in the more solid phase.

Those physical properties are determined by different proteins regulating the larger scale behaviour of the cortex. We can classify main ones as follow:

1. Nucleators creating new branches of filaments.

2. Regulators of the assembly clustering filaments.

3. Crosslinkers and bundlers attaching filaments. Bundles tend to produce less random or more organised networks of actin filaments than crosslinkers.

The cortex being under the plasma membrane we expect some friction resulting from the attachment of the cortex to the lipid bilayer. The viscoelasticity is described more elastic for short timescales (<1 min) and more like a viscous flow for larger timescales. The description of the cortex depends on the force applied at different frequencies.

1.2.5 Membrane ruffles

Ruffles are membrane folds looking structures initiated by actin filament polymerisation and participate in cell active processes. They can be seen as a prolongation of the cell to move or catch objects in phagocytosis for example. The actin by polymerising under the lipid membrane bilayer. Those actin driven ruffles have an estimated thickness of a few hundred nanometres and different distributions [5]. Lamellipodia appears to have a more distributed size on the contrary filopodia and ridges have a lower spread of the thickness values.

1.3 Endocytosis and channel diffusion

The first observations of microorganisms were made by Leeuwenhoek in the 17th century using a microscope but it is in the early 20th century that Ilya Metchnikov was awarded the Nobel Prize in Physiology or Medicine in 1908 for his work on immunity and more precisely phagocytosis [16]. We distinguish endocytosis processes involving actin like phagocytosis (reviewed in [38])(reviewed in [38]), macropinocytosis and others like clathrin-mediated or caveolin mediated endocytosis.

1.3.1 Phagocytosis

The way a cell can absorb from its environment elements can differ depending on the characteristics of the target. This leads to a variety of processes performed by the cell and involving more or less a large reshaping of the cell membrane through signaling pathways. For rigid targets under $0.5\mu m$ endocytosis receptor

mediated and translocation are commonly observed. On the other hand larger targets requiring more energy and deformations will go through more elaborated mechanisms with an initial step of cup formation and the pseudopod extension all around the target. The process is active and requires the help of the actin cytoskeleton to close the bag wrapping the target called phagosome.

1.3.2 Clathrin and caveolae mediated endocytosis

Clathrin and caveole mediated endocytosis use an invagination by the membrane to the inside of the cell and require the mediation of a protein coated on the vesicle. Caveolae mediated endocytosis creates vesicles of $50-60nm$ and $120nm$ for clathrin mediated endocytosis (reviewed in[15]).

1.3.3 Macropinocytosis

Macropinocytosis consists in the uptake of fluid where other tiny particles can be present inside a macropinosome. Macropinocytosis shares with phagocytosis the actin dependency but does not require any coating, obviously for a fluid, that are usually present in pahgocytosis with antibody coating or clathrin mediated endocytosis (reviewed in [32]). A mechanism proposed as an archaic version of phagocytosis where osmosis reducing the volume of the cell for a constant membrane surface would increase the number of ruffles and with random fluctuations of the shape engulfs a volume of fluid. The difference with macropinocytosis is the actin role creating ruffles making it an active process.

1.3.4 Active and passive diffusion

For tiny particles with a given concentration in the surrounding of the membrane can occur in a passive way following the gradient of concentration from more concentrated to less concentrated creating a flux following Fick's law. Another type of diffusion is through channels in the membrane requiring energy making it an active process and selecting the molecules to cross the membrane. The scale of the molecules or particles concerned by diffusion are not at the centre of our work.

1.3.5 Target shape, size and rigidity influence on endocytosis

The way phagocytosis takes place is observed to change based on the geometrical and elastic properties of the target. IgG (an antibody) coating is commonly used in experiments on the targets to make the macrophage engage engulfment. Outside of coating the size plays a role in the way a target is engulfed. A bead that is equivalent in size to the macrophage may be impossible to engulf or rarely and we would rather see the phagocytic cup unable to form completely. In terms of mechanosensitivity the cell reacts differently with elasticity of the target. Too rigid targets ($>$ 10 MPa) are believed to be too stiff to indent

Table 1.1: Table of the estimated outcome for bead size related to the highest uptake.

Reference	Preferred radius estimation (μm)
[36]	0.75
[7]	1.25
[23]	No preferred size
[5]	0.5

(reviewed in [38]). Too soft materials would be too soft to be "felt" by the cell and create the necessary signalling. The curvature plays a role too based on the speed of internalisation and phagocytic cup formation when we point the highest curvature point of an ellipsoid shape object first instead of a spreading when the flatter surface is faced[6]. Highly curved area of a target seem to help in the phagocytic cup formation and success in engulfment compared to sphere or more regularly curved shapes (smooth) (reviewed by [15]). Even if there is enough evidence to notice an influence of shape, size and stiffness it is much more complicated to isolate the effect of each one separately but a size increase appears to have more impact in reducing internalisation compared to decreasing stiffness [13]. We also point out that in the case of a sphere size and shape are simply related: increasing the size reduces the curvature and vice versa.

1.4 Observations from the literature

Experiments from the literature (given in Table 1.1) have studied the internalisation of beads by a population of macrophages to count the number of beads internalised by macrophage for different sizes of beads. It appears that for a certain range size we have a higher intake of beads per macrophage suggesting an easier process of internalisation that we can understand as physicist as a lower amount of energy needed for the uptake. This will naturally lead us to investigate the energy associated with membrane reshaping. As said earlier in this introduction the size is not the only parameter determining the outcome of an engulfment and its success rate (see section 1.3.5). Outside of considering a single event intake we have the probability of contact between a bead and a macrophage since it is an experiment involving a population of cells surrounded by beads. The combination of all those potential parameters requires some caution when discussing and comparing our results with the experiments.

1.5 Overview on the next chapters

We can now introduce the next chapters where we model three different cases. In chapter 2 we study the engulfment of a bead and the size effect on the deformation energy of the membrane. We will consider a minimum of energy as

a preferred size. The cortex will be also a point of interest for high curvature case. We also combine probabilities between probability of contact and single engulfment probability with thermal fluctuations. Finally we open a discussion on the results obtained accompanied by elements from the literature. Chapter 3 is dedicated to the time evolution of engulfment. A feedback model is proposed for the phagocytosis last half of engulfment for a spherical target including viscous properties and force generated by actin around the sphere. After that, chapter 4 is about nucleus migration or constriction crossing and the outcome of it depending on geometrical parameters like nucleus and constriction size to elastic and force generation properties. The idea is to be able to estimate the possible success or not of crossing given the input conditions. Finally we will summarise the results obtained and give possible outlooks for each chapter.

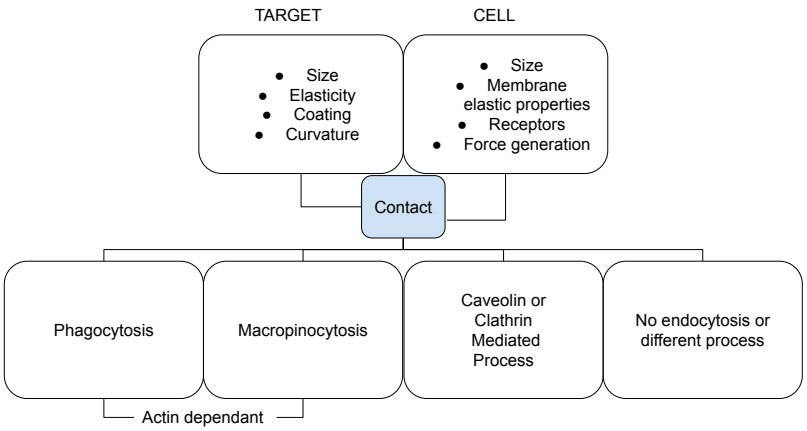

Figure 1.5: Possible outcomes based on the initial cell and target characteristics.

Chapter 2

Phagocytosis: Energy and take up probability

In this first section we aim to describe the membrane in terms of energy variations after reshaping. The most common energy formulation used is the one derived by Helfrich in 1973[17]. It is very close to the thin plate energy bending formulation for the bending term given in [20]. We can make the derivation from a microscopic description of the membrane[31]. Once we are able to describe the energy of a deformation we investigate the possibility of an ideal configuration of size and shape as suggested by other works [14][26][5]. In a second time we focus on the cortex and a possible limitation in bending from excluded volume interaction giving rise to an ideal size of bead that we discuss further. Finally we end this chapter with the combination of a contact probability between cell and target with the probability of reaching halfway of engulfment. We will conclude by summarising all the approaches considered and discussing them with results from the literature.

2.1 Lipid bilayer deformation energy

The lipid bilayer is represented as two layers of self assembled lipids interacting and at an equilibrium phase. The membrane can be stretched or bent leading to an increasing of energy.

To describe the bending of a surface in a 3D space we have two main curvatures. We need to introduce two scalars: the Gaussian curvature and the mean curvature respectively to calculate the energy associated with a bending .

The integrated curvature energy per surface area is given by eq.2.1[25]:

$$E = \int (2\kappa(H - H_0)^2 + \gamma + k_G K)dA + \int \Delta P dV. \tag{2.1}$$

1. κ is the bending modulus that has the dimension of an energy.
2. $H = \frac{c_1+c_2}{2}$ and H_0 are respectively the average curvature and the spontaneous curvature. The spontaneous curvature can be different from zero.
3. γ is the surface tension constant with the dimension of energy per surface area.
4. K is the Gaussian curvature i.e. $K = c_1 c_2$.
5. ΔP is the difference in pressure between the two sides of the membrane. We assume that during phagocytosis the difference of pressure before closing of the phagosome can be neglected and that we have an equilibrium.

We have the following energy per unit of surface isolating the contribution from bending

$$e_b = \frac{k_b}{2}(H - H_0)^2. \tag{2.2}$$

The curvature may be negative or positive depending on which side is bent which is a matter of convention. The most important is to keep the same convention through calculations. To illustrate the curvatures we can give few examples of 2d surfaces with their respective curvatures (see fig.2.1).

1. The simplest one being the plane with zero curvatures: $c_1 = c_2 = 0$
2. The sphere of radius R with $c_1 = c_2 = \pm\frac{1}{R}$
3. The cylinder with two different main curvatures. On the longitudinal axis z we have $c_1 = 0$ and $c_2 = \pm\frac{1}{R}$ with R the radius of the cylinder.
4. Another shape is the catenoid with $c_1 = -c_2$. The interesting fact is that it gives $H = 0$ which is the same mean curvature as the plane in terms of bending energy.

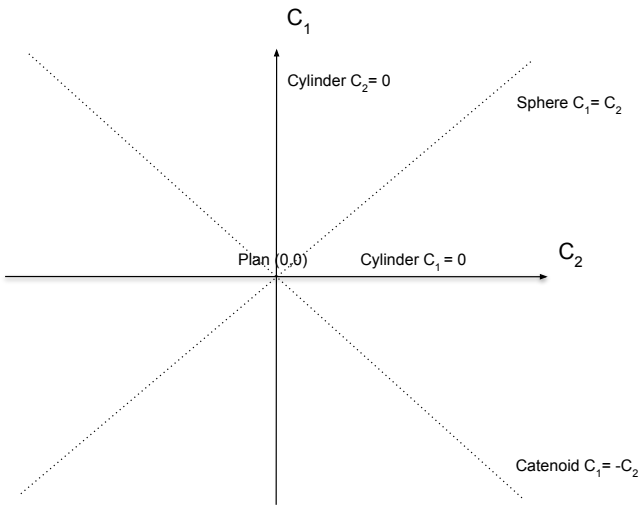

Figure 2.1: Possible shapes for a given set of value (c_1,c_2) as the two main curvatures.

2.2 Helfrich energy for different deformations

In order to describe the energy changes we need to explain first the representation of the cell we consider. Experimentally the cell has no regular shape and we can only estimate a volume based on frames taken. For the next parts of our work we consider the cell as a sphere to simplify the situation and because it is the closest ideal shape we can consider. In case we would have to refer to the experiments where the volume is given we may use an estimated radius of the cell

$$R_0 = \left(\frac{3}{4\pi}\right)^{\frac{1}{3}} V_0^{\frac{1}{3}}. \tag{2.3}$$

We start by calculating the squared term contribution involving the curvature which is defined by

$$E_1 = 2\kappa \int dA\,(H - H_0)^2 \tag{2.4}$$

with H the average curvature

$$H = \frac{c_1 + c_2}{2}. \tag{2.5}$$

c_1 and c_2 are the main curvatures of the surface and for a sphere of radius R_0 the mean curvature is

$$H_0 = \frac{2}{2R_0} = \frac{1}{R_0}. \tag{2.6}$$

We consider the engulfment of a sphere with radius R by a macrophage of radius R_0 represented as a sphere (see fig.2.2).

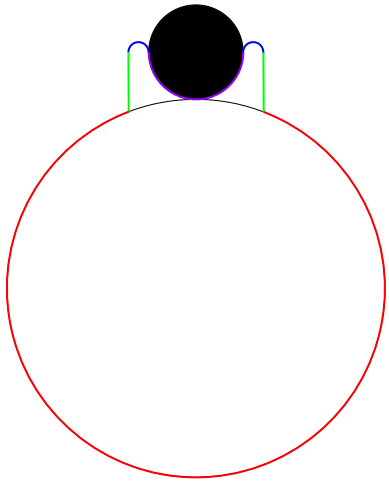

Figure 2.2: 2D representation of the sphere with radius R engulfed by the membrane. In red the undeformed shape. The blue section is a 2d view of the torus with a small radius e and R for the larger radius (R)

2.2.1 Sphere. Part 1

We calculate the total energy for the curvature in purple forming the cup fitting the bead (see fig.2.2) that corresponds in absolute value to $\frac{1}{R}$ since we consider that it follows the shape of the sphere until the point of phagocytosis

$$E_{B1} = 2\kappa 2\pi R^2 \left(\frac{1}{R} + \frac{1}{R_0}\right)^2 = 4\pi\kappa \left(1 + \frac{R}{R_0}\right)^2. \tag{2.7}$$

We introduce a nondimensional parameter $r = \frac{R}{R_0}$ that characterises the ratio between the macrophage and the target and make it easier to manipulate

for any macrophage size. We limit our study to $R < R_0$, i.e. $r < 1$. The energy can be rewritten as

$$E_{B1}(r) = 4\pi\kappa\,(1+r)^2\,. \tag{2.8}$$

The eq.2.8 has no minimum for $r > 0$ (see fig.2.3) that is irrelevant in terms of physics. The smallest bead we consider must be larger in radius than the thickness of the lipid bilayer to keep the validity of the equations.

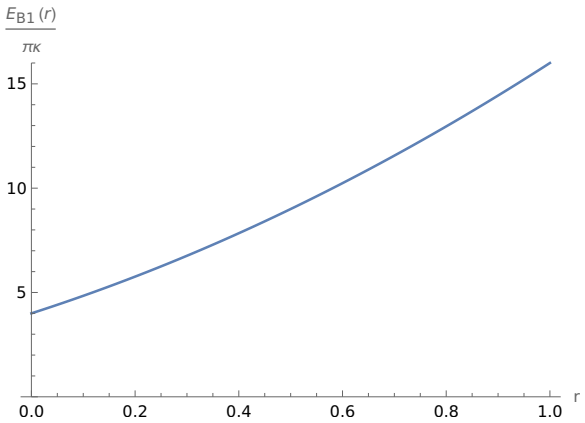

Figure 2.3: Increasing energy in units of $\pi\kappa$ for the spherical shape with r. It is a monotonous increasing energy when increasing size r.

2.2.2 Cylinder. Part 2.

The average curvature for the cylinder in green (fig.2.2) can be written

$$H = \frac{c_1 + c_2}{2} = \frac{1}{2(R+2e)}, \tag{2.9}$$

where the variable e is the radius of the the circle in blue corresponding to a cut of the torus on fig.2.2. In the case where $R >> 2e$ the average curvature tends to $H \to \frac{1}{2R}$ we have

$$E_{B2} = \pi\kappa\,(1-2r)^2\,. \tag{2.10}$$

The curvature of the cylinder is positive following the convention $H_0 = \frac{1}{R_0}$. The result is shown in fig.2.4.

2.2.3 Energy for the torus. Part 3.

The torus [24] has a constant curvature c_1 on one direction corresponding to $\frac{1}{e}$ and a changing curvature for c_2 given by

$$c_2 = \frac{\cos u}{R_t + e\cos u}, \tag{2.11}$$

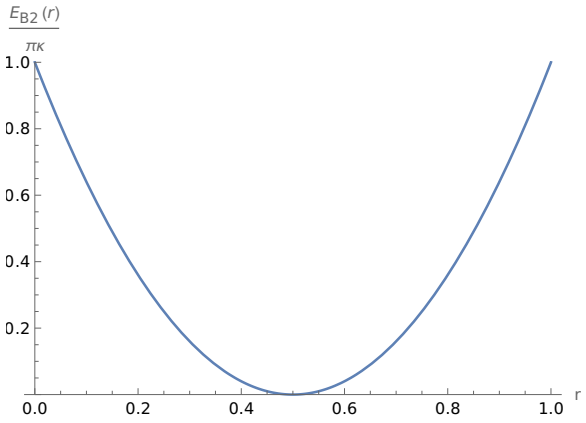

Figure 2.4: Increasing energy in units of $\pi\kappa$ for the cylinder shape with r. It has a minimum for $r = 0.5$.

with u the angle on the circle of the cross section of the torus. We have to be careful with the large radius R_t defined in the torus of revolution as it corresponds to $R + e$ in our case. By introducing $R_t = R + e$ we have

$$c_2 = \frac{\cos u}{R + e(1 + \cos u)}. \tag{2.12}$$

The surface of half a torus can be expressed as

$$S_T = 2\pi^2 Re \tag{2.13}$$

and the average curvature H is given by

$$H = \frac{c_1 + c_2}{2} = \frac{1}{2}\left(\frac{1}{e} + \frac{\cos u}{R + e(1 + \cos u)}\right). \tag{2.14}$$

Case $e << R$.

In the case where e is very small compared to R and R_0 we approximate H as

$$H_{Torus} \approx \frac{1}{2e}, \tag{2.15}$$

we want to minimise the energy with respect to e. The bending energy contribution for the half torus and the cylinder from equation 2.10 are the expressions showing explicitly e. We start by giving the curvature term for the torus

$$E_{B3} = 2\kappa \frac{1}{4e^2} 2\pi^2 eR = \pi^2 \kappa \frac{R}{e} \tag{2.16}$$

and the contribution from the surface tension

$$E_{S2} = \gamma S_2 = \gamma 2\pi^2 Re. \tag{2.17}$$

The energy contribution from the cylinder may be neglected since $e << R$. The radius of the cylinder is approximated as $R + 2e \approx R$. We can finally write the total energy with terms showing e explicitly

$$E_{S2} + E_{B2} = 2\pi^2 \gamma R e + \pi^2 \kappa \frac{R}{e}, \tag{2.18}$$

the derivative of eq.2.18 with respect to e gives

$$\frac{\partial (E_{B2} + E_{S2})}{\partial e} = \pi^2 R (2\gamma - \frac{\kappa}{e^2}) = 0. \tag{2.19}$$

We finally deduce an expression for e given by eq.2.20.

$$\boxed{e^* = \sqrt{\frac{\kappa}{2\gamma}}}, \tag{2.20}$$

in terms of membrane folding space of the pseudopod surrounding the target it is the diameter $2e$ given by

$$2e^* = \sqrt{\frac{2\kappa}{\gamma}}. \tag{2.21}$$

We notice that a similar result for eq.2.21 is given by [40] for the minimum radius size of the spherical target to trigger endocytosis. We can give an estimate of the spacing $2e^*$ using values of κ and γ from the literature. The value of κ seems to change from $4 \times 10^{-20} J$ (or $10kT$) to $16.10^{-20} J$ (or $40kT$). A good review on the estimations of the bending modulus can be found in [3]. The measured surface tension is estimated to be around $2.07 mN.m^{-1}$. Using those values we have

$$2e^* \approx 2\sqrt{\frac{16.10^{-20}}{4.10^{-3}}} \approx 12nm, \tag{2.22}$$

as a point of comparison protrusions are around few hundred nanometres which seems an order of magnitude higher compared to the result in eq.2.22.

The bending modulus seems to be hard to determine since the estimated values of κ change depending on the measurement method i.e. numerical, experimental or theoretical. The value of κ and γ are not completely uncorrelated.

A possible origin to this difference is the fact that the view of a perfectly organised lipid bilayer in practice for a cell is wrong. The proteins interacting with the membrane and inhomogeneous element added could change the physical properties of the membrane bilayer in vivo. Taking into account "defects" in the bilayer structure may give a higher estimate of the bending modulus and surface tension.

Moreover κ and γ are two parameters that are indirectly related and can change both at the same time meaning that they are not completely independent. Since we have a ratio of both parameters one can expect a possible simpler expression of e^*. Knowing also that estimations are made for ideal situations where the lipid bilayer is described as pure and contrasts with the cell membrane including the attached cortex under it changes the response and makes it potentially more difficult to bend giving an effective $\kappa_{eff} > \kappa$.

Following the thin plate or shell theory the bending modulus is given by

$$\kappa = \frac{Eh^3}{24(1-\nu^2)} \tag{2.23}$$

with the following parameters:

- E: Young modulus.
- ν: Poisson's ratio describing the compressibility.
- h: The thickness of the shell or plate.

The expression shows how the bending modulus is affected by the thickness h. Taking a value of h ten times higher will multiply the bending modulus by a factor 10^3. Referring to eq.2.20 we take the square root ($\sqrt{1000} \approx 32$). This increases the previous value of $2e$ to $2e \approx 384nm$ which is larger than the previous estimation and closer to estimated thicknesses of protrusion measured in experiment [5].

Total energy for the sphere

We can finally sum the three contributions for the halfway configuration (see fig.2.2) in order to compare it with the nearly full engulfment. We assume that $R + e \approx R$ and have

$$E_{half} = 2\kappa \left(2\pi \left(1 + \frac{R}{R_0} \right)^2 + \pi^2 \frac{R}{e} + \frac{\pi}{4} \left(1 - \frac{2R}{R_0} \right)^2 \right) + \gamma(2\pi^2 Re + 2\pi R^2 + 2\pi R^2), \tag{2.24}$$

this energy is to compare with the energy at nearly full engulfment where we close with a catenoid before the fusion of the membrane. By removing the torus and adding the two spherical part fully covering the bead we obtain

$$E_{full} = 2\kappa \left(4\pi \left(1 + \frac{R}{R_0} \right)^2 + \frac{\pi}{4} \left(1 + \frac{2R}{R_0} \right)^2 + 2\pi \left(1 - \frac{R}{R_0} \right)^2 \right) + \gamma(4\pi R^2 + 2\pi R^2 + 2\pi R^2). \tag{2.25}$$

We give the expression of the difference between the energy of full engulfment and half way engulfment $\Delta E = E_{full} - E_{half}$ with eq.2.26.

$$\Delta E = 2\kappa \left(2\pi \left(1 - \frac{R}{R_0} \right)^2 - \pi^2 \frac{R}{e} \right) + \gamma(4\pi R^2 - 2\pi^2 Re) \tag{2.26}$$

$$\Delta E = 2\pi\kappa \left(2\left(1 - r\right)^2 - \pi \frac{R}{e} \right) + 4\pi\gamma R^2 (1 - \pi \frac{e}{2R}) \tag{2.27}$$

Taking the assumption from eq.2.22 the term $\pi \frac{R}{e}$ dominates since $r < 1$. Taking also $\frac{\pi e}{2R} << 1$ gives

$$\Delta E = 4\pi\gamma R^2 - 2\pi^2 \kappa \frac{R}{e}, \tag{2.28}$$

taking the situation for which $\Delta E = 0$

$$R = \frac{\pi\kappa}{2\gamma e}. \tag{2.29}$$

Using result from eq.2.20 we have the radius R_Δ for which $\Delta E = 0$ and changes sign. For $R > R_\Delta$ we have $\Delta E > 0$ and $\Delta E < 0$ in the case $R < R_\Delta$

$$R_\Delta = \pi\sqrt{\frac{2\kappa}{\gamma}}. \tag{2.30}$$

The expression given by eq.2.30 gives the minimum radius bead for which full engulfment has a higher energy in terms of curvature energy and surface tension combined. It means that for a radius $R < R_\Delta$ the configuration of full engulfment, just before the closing of the engulfment cup wrapping the target, has a lower energy than the configuration before. The extra energy between half engulfment and full engulfment, when $R < R_\Delta$, can possibly be released in the form of thermal energy for example.

2.3 Bending energy around a spherocylinder

After the sphere shape we investigate a more complex structure to the changes we can expect from a shape with different symmetries. We can think of the initial sphere that we cut in half and introduce a cylinder of length L to connect them. We end up with a spherocylinder or a pill shape (see fig.2.5) that the macrophages will engulf. We can identify two shapes:

- The cylinder in the middle with radius R at the basis and length L. The two principal curvatures of a cylinder in absolute value will be 0 and $\frac{1}{R}$.
- Two semi-spheres in order to have a close surface with radius R too. For the sphere we have two same main curvatures $1/R$ in absolute value.

This shape ensures the closed of the surface around the boundary between the spherical shape and the cylinder. The first derivative is also continuous. One of the main curvatures won't be continuous jumping from 0 to $\frac{1}{R}$. The area of the cylinder is given by

$$S_1 = 2\pi RL, \tag{2.31}$$

knowing the two main curvatures we can calculate the energy related to the average curvature

$$H = \frac{c_1 + c_2}{2} = \frac{1}{2}\left(0 - \frac{1}{R}\right) = -\frac{1}{2R}. \tag{2.32}$$

The total energy may be split into two separate contributions. The one from the cylinder and twice the energy of the hemisphere

$$E = E_{Cylinder} + E_{Hemisphere}, \tag{2.33}$$

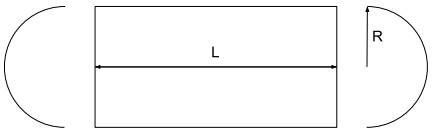

Figure 2.5: 2d representation of a spherocylinder

we calculate the contribution from the cylinder

$$E_{Cylinder} = 2\kappa \left[2\pi RL \left(\frac{1}{2R} + \frac{1}{R_0} \right)^2 \right] = \pi\kappa \frac{L}{R} \left(1 + \frac{2R}{R_0} \right)^2 \tag{2.34}$$

and give the bending energy for the hemispheres

$$E_{Hemisphere} = 8\pi\kappa \left(1 + \frac{R}{R_0} \right)^2 . \tag{2.35}$$

By summing the two energies we have the total energy corresponding to the bending. We introduce $r = \frac{R}{R_0}$ and $l = \frac{L}{R_0}$ the total energy

$$E = \pi\kappa \underbrace{\left[8\left(1+r\right)^2 + \frac{l}{r}\left(1+2r\right)^2 \right]}_{\text{f(r,l)}} . \tag{2.36}$$

The figure 2.6 shows the function $f(r, l)$ for different values of l showing the evolution and position of the minimum.

Derivation of the minimum

From the previous section we differentiate the function $f(r, l)$ to find the position $r^*(l)$ of the minimum. We start from $f(r, l)$ given by

$$f(r,l) = \left[\frac{l}{r}\left(1+2r\right)^2 + 8\left(1+r\right)^2 \right], \tag{2.37}$$

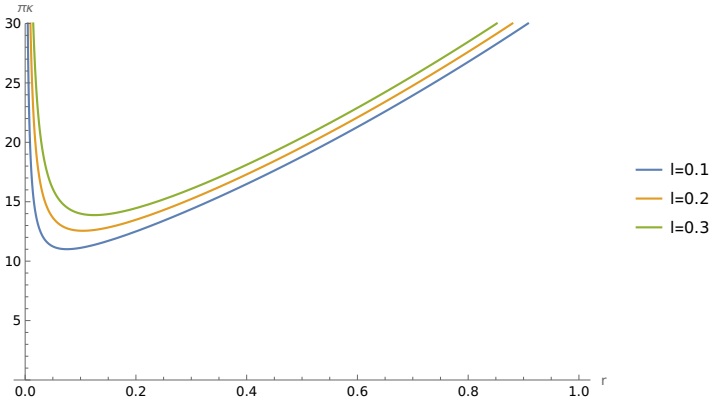

Figure 2.6: Function f (see eq.2.36) for different values of l. We can see a minimum $r > 0$ showing up for $l > 0$.

we differentiate with respect to r eq.2.37 to obtain

$$\frac{df}{dr} = 16(1+r) - \frac{l}{r^2}(1+4r^2+4r) + 4\frac{l}{r}(1+2r) \tag{2.38}$$

and set the equation $\frac{df}{dr} = 0$ to solve

$$16(1+r) - l(4+\frac{4}{r}+\frac{1}{r^2}) + 4l(2+\frac{1}{r}) = 0. \tag{2.39}$$

We end up with a polynomial to solve

$$16r^3 + (4l+16)r^2 - l = 0, \tag{2.40}$$

the solution $r^*(l)$ for eq.2.40 is solved using Mathematica and showed in fig.2.7. The limit $l >> 1$ from this model says that for any length L of the spherocylinder the radius minimising the bending energy will always be $r^* < 0.5$ because of the limit when $r^*(l >> 1) \to 0.5$. A potential comparison with existing spherocylindrical shape in the biological world is with bacteria like E.coli.

2.4 Cortex model

Experimentally the available data and observations from [36][6] indicates a higher intake of beads by macrophages when exposed to a population of beads with in a certain range size of few hundred nanometres. Until now we have used the Helfrich bending energy of a lipid bilayer to quantify the energy needed for the reshaping necessary for engulfment. This approach neglects the possible effect from the cortex contribution positioned under the lipid bilayer and the fact that the range we look at is close to the thickness of the membrane lipid bilayer and cortex combined. The cortex thickness is of the order of few $100nm$

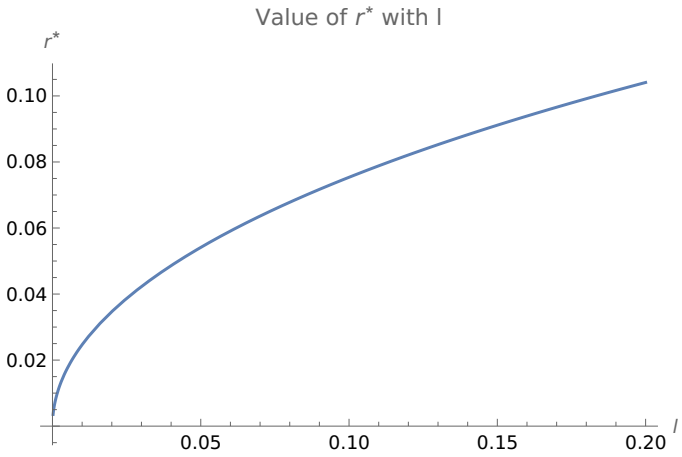

Figure 2.7: Evolution of r^* minimising the energy of bending with respect to the length l. We have $r^*(l \to \infty) \to \frac{1}{2}$.

and the range of size of bead radius is the same.

We propose in the following section a description of the cortex energy contribution to the bending. It is a way to highlight the possible important role of the cortex in the size and/or shape effect on phagocytosis.
We aim for a simple representation of the cortex composed of interacting elements (actin filaments, proteins,...) with an average spacing. From there we find the effect of the curvature on the average spacing.
In a second time we introduce an energy potential that describes an interaction of unknown nature with free parameters that we discuss later.

In the following section we focus on the small range beads that we are interested in which means in the range of few $100nm$ in radius.

We represent the cortex as a structured network under the membrane lipid bilayer (see fig.2.8) with average distance h between the solid elements in it like the filaments and a cortex thickness w. The bending follows a curvature $\frac{1}{R}$ with R the radius of the bead. Another supposition is that the deformation doesn't change noticeably h.
We aim to find d (see fig.2.9) the new average distance as we bend change the curvature with different bead radii R as a function of the other geometrical parameters R, w and h. d is the shortest distance that we take as the most relevant along the transversal axis of the cortex that we use to quantify the energy. Since we consider an excluded volume type interaction the smaller the distance d the higher will be the energy.

We draw a circle representing the spherical target in 2d and larger one with a radius $R + \frac{w}{2}$. We take two lines separated by a distance h as shown in fig.2.9.

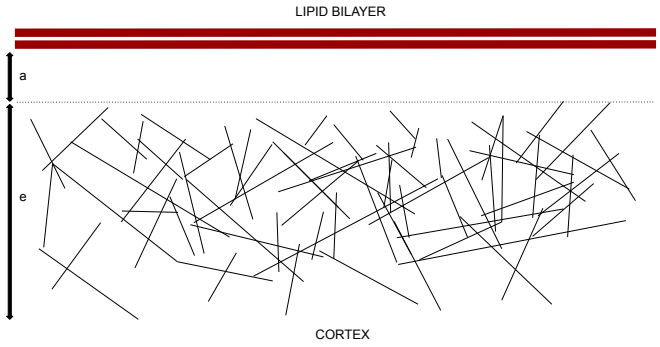

Figure 2.8: Representation of the lipid bilayer with the cortex just under.

We have

$$\frac{d}{2R} = \frac{h}{2(R + \frac{w}{2})} \tag{2.41}$$

and deduce $d(h, w, R)$ given by

$$d = \frac{h}{1 + \frac{w}{2R}}. \tag{2.42}$$

We notice that for beads of large size compared to the thickness of the membrane-cortex elastic sheet $d = h$ which leads to the flat case but for our study we remain in our case where the the size of the bead is of the same order as the thickness of the cortex. We should mention also that we can keep in mind the possible gap between the cortex and the lipid bilayer. The following transformation can be done to include this gap. In practice it like a new effective radius (see eq.2.43). It is like having a larger radius in the calculation

$$R \to R + a, \tag{2.43}$$

the consequence when reading the data would be to keep in mind that results may be shifted. The estimation of this gap experimentally (reviewed in [8]) indicates that one should be aware that any result regarding R may be shifted by the size of this gap a(see fig.2.8).

2.4.1 Excluded volume interaction.

We assume a general form of an interaction between the cortex elements describing the excluded volume given by

$$E(d) = \frac{A}{d^{\nu}}, \tag{2.44}$$

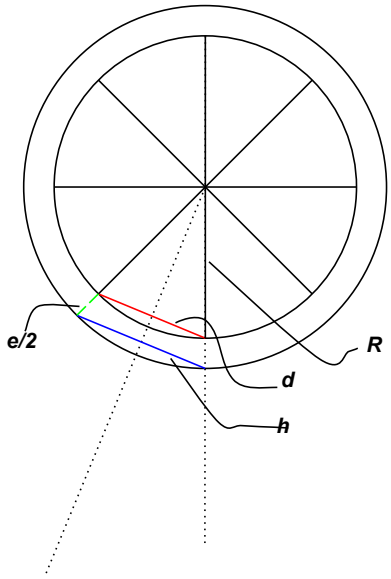

Figure 2.9: Representation of the membrane-cortex complex surrounding the spherical bead. w is the total thickness. R the radius of the bead. h is the average spacing between the elements of the cortex.

we consider mainly the leading order of this interaction since one could in a general case write down the sum of all the powers as a serie of all negative powers. We define A as a constant that can depend on different parameters in the actin network like a random process (temperature) for example, chemical reactions or even concentrations. We will see later that for our purpose and without stretching or surface tension from the membrane it is not relevant for our final result. The range of the interaction associated with ν is more complex to link with an experimental parameter than the thickness of the cortex that is an observable which can be estimated. Replacing the distance with eq.2.42 in eq.2.44 we obtain

$$E_s(R) = \frac{A(1+\frac{w}{2R})^\nu}{h^\nu}. \tag{2.45}$$

For a single element of surface dS we have 4 interactions for a square lattice on the surface. We integrate over the surface corresponding to the spherical bead engulfed by the cell. We have the energy given by

$$E(R) = \frac{16\pi R^2 A(1+\frac{w}{2R})^\nu}{h^\nu}, \tag{2.46}$$

the expression in eq.2.46 without adding any other term to the total energy has a minimum that we investigate in the next section.

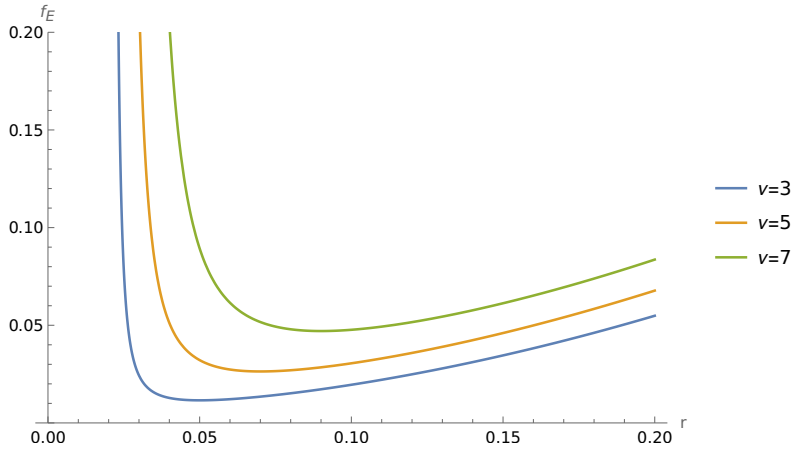

Figure 2.10: Minimum position for $f_E = R^2 \frac{(1+\frac{w}{2R})^\nu}{h^\nu}$ changing with ν and $\frac{w}{R_0} = 0.02$.

2.4.2 Minimum energy

We start from the expression in eq.2.46 and introduce the parameter given by

$$\epsilon = \frac{w}{R_0}, \tag{2.47}$$

to simplify we introduce a new constant $C = \frac{24\pi A}{h^\nu}$ and the set of variables (r, ϵ). We can rewrite eq.2.46 into (see fig.2.10 and fig.2.11)

$$E_1(r) = Cr^2 \left(1 + \frac{\epsilon}{2r}\right)^\nu. \tag{2.48}$$

We differentiate eq.2.48

$$\frac{dE_1}{dr} = \frac{2r}{\left(1 - \frac{\epsilon}{r}\right)^\nu} - \frac{\nu\epsilon}{\left(1 - \frac{\epsilon}{r}\right)^{\nu+1}} = 0, \tag{2.49}$$

with respect to r to find the minimum of energy. We notice that the only physical parameters affecting the position of the minimum r^* are ν and w. We simplify eq.2.49

$$2r + \epsilon - \frac{\epsilon\nu}{2} = 0 \tag{2.50}$$

to find the expression of r^* given by

$$r^* = \frac{\epsilon}{2}\left(\frac{\nu}{2} - 1\right). \tag{2.51}$$

In our model e is the thickness of our cortex. For higher values of ν we expect a higher value of $R^* = R_0 r^*$. We notice also that the minimum of energy or maximum of take-up is expected to be always greater than e meaning that the

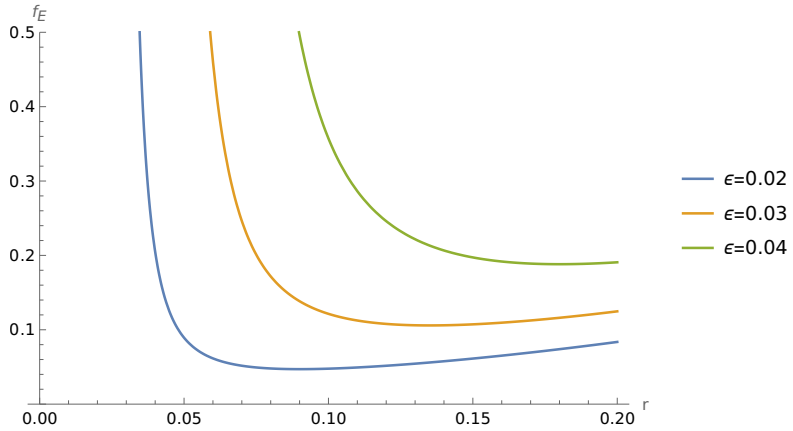

Figure 2.11: Minimum position changing for different ϵ and $\nu = 7$.

thickness of the cortex should always be smaller than the maximum of uptake corresponding radius following this model. Assuming that ν is an integer we deduce that to have a solution we need

$$\nu \geq 3. \tag{2.52}$$

Since we are working in a 3d system it means that the short range interaction is necessary to have a solution and see this effect.

2.4.3 Effect from stretching energy and surface tension

In the following section we aim to study the potential effect of tension and stretching on the curvature energy and the location of a minimum.

Surface tension

As an example we take the result from section 2.4.2 to show how surface tension can influence the location of the minimum. We give the sum of both energies including surface tension

$$E = Cr^2 \left(1 + \frac{\epsilon}{2r}\right)^{\nu} + 4\pi\gamma R^2, \tag{2.53}$$

we can rewrite the surface tension term and eq.2.53 into

$$E = Cr^2 \left(1 + \frac{\epsilon}{2r}\right)^{\nu} + 4\pi\gamma R_0^2 r^2. \tag{2.54}$$

To compare the bending energy and surface tension energy contribution we introduce a dimensionless parameter

$$\omega_1 = \frac{4\pi\gamma R_0^2}{C} \tag{2.55}$$

and we introduce $E_C = \frac{E}{C}$ in

$$E_C(r, \epsilon, \nu, \omega_1) = r^2 \left(1 + \frac{\epsilon}{2r}\right)^{\nu} + \omega_1 r^2, \tag{2.56}$$

the effect of w_1 can be seen in fig.2.12 and how the position of the minimum to the left of the r-axis. The addition of surface tension is changing the location to the left of the r-axis (see fig.2.12).

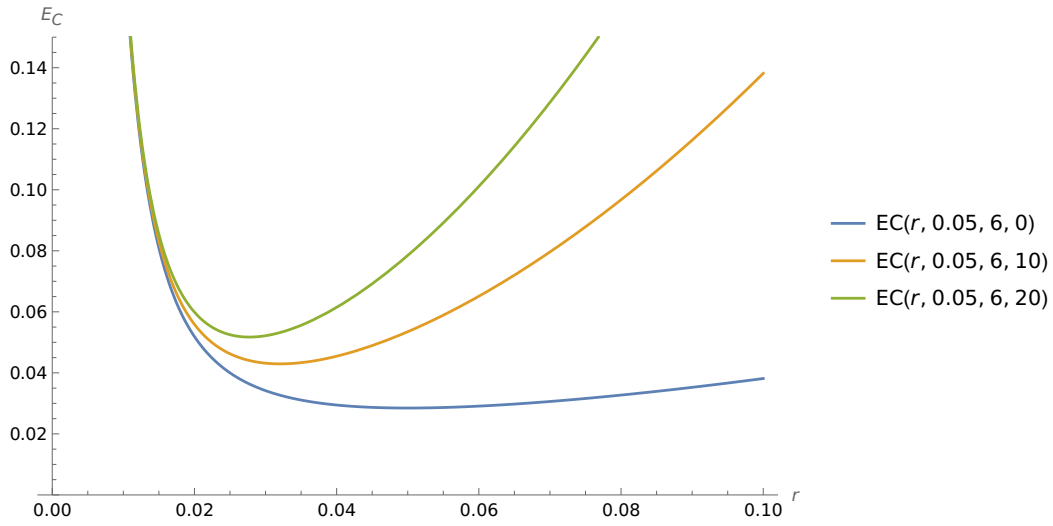

Figure 2.12: Effect of surface tension on the location of the minimum for different values of ω_1.

Stretching

Knowing the extra surface needed and the maximum stretchability we can estimate the potential engulfment possible without any extra patches of surface. We have

$$4\pi R^2 = 4\pi k R_0^2, \tag{2.57}$$

k is the proportion of maximum stretching. For example 4% is $k = 0.04$. We estimate the maximum value of R possible with pure stretching

$$R_{max} = \sqrt{k} R_0, \tag{2.58}$$

in another form in terms of ratio we have

$$\frac{R_{max}}{R_0} = r_{max} = \sqrt{k}. \tag{2.59}$$

The stretching energy with ΔA the extra area required and A_0 the initial area

$$E = \frac{K_s}{2} \frac{\Delta A^2}{A_0}, \tag{2.60}$$

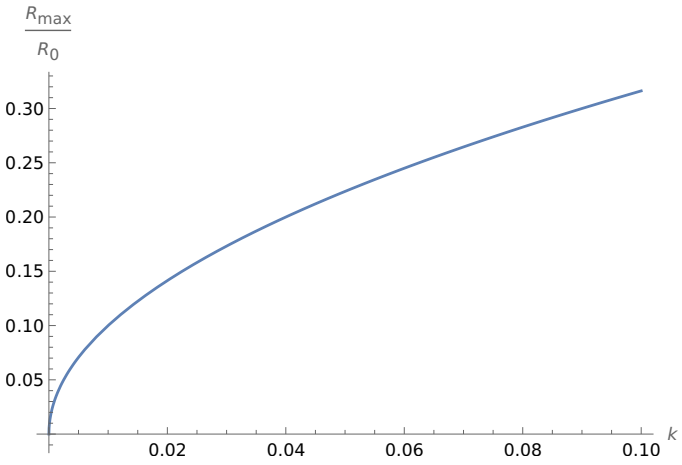

Figure 2.13: Maximum radius with pure stretching.

we have the following total energy

$$E = Cr^2\left(1+\frac{\epsilon}{2r}\right)^{\nu} + \frac{K_s}{2}\frac{\Delta A^2}{A_0}. \tag{2.61}$$

Written as a function of R with $\Delta A = 4\pi R^2$

$$E(R) = Cr^2\left(1+\frac{\epsilon}{2r}\right)^{\nu} + \frac{2\pi K_s}{R_0^2}R^4, \tag{2.62}$$

we introduce $\omega_2 = \frac{2\pi K_s R_0^2}{C_1}$ and $E_{C_2} = \frac{E}{C}$ and obtain (see fig.2.14)

$$E_{C_2} = r^2\left(1+\frac{\epsilon}{2r}\right)^{\nu} + \omega_2 r^4. \tag{2.63}$$

2.5 Probability of contact combined with engulfment

In this section we include the probability of contact between a macrophage and a spherical bead combined with the probability of forming a phagocytosis cup with Helfrich energy. We assume that we have N_M macrophages and N spherical targets in a given volume V_0. We make the following assumptions:

- The density of beads is larger than the number of macrophages or we assume that we have a reservoir keeping the density unchanged.
- The targets are small enough to neglect the targets already internalised by the macrophages. It is to avoid the fact that after many internalisation the macrophage may be limited by the surface and volume availability to engulf.

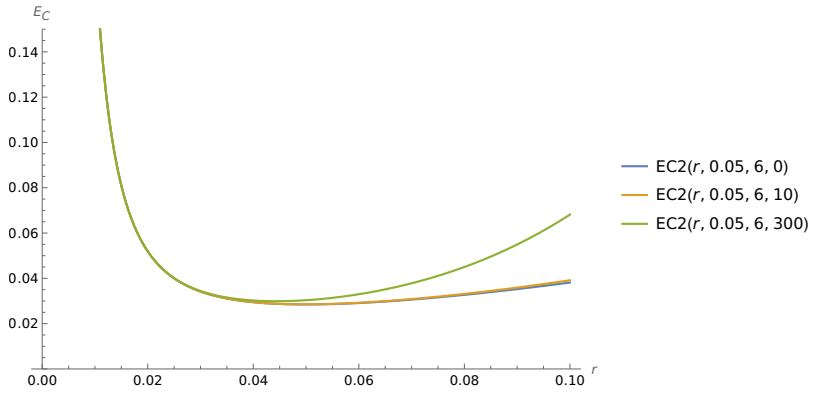

Figure 2.14: Effect of stretching on the minimum for different values of w_2. As we increase the stretching modulus through ω_2 we observe that the location of the minimum become smaller and tends to the left of the r-axis.

- We exclude too extreme curvatures like a flat surface or spikes in terms of curvatures. This is to assume that anytime a macrophage encounters a targets a phagocytic cup is formed.
- The bead is small enough that it does not require stretching or a negligible amount compared to the bending energy.

We assume that a macrophage during the experiment has a volume V with N targets available around it and the distribution of targets and macrophages uniform. R is the radius of the target and R_0 the radius of the cell. The probability to find a target is given by

$$P_1 = \frac{\text{Volume occupied by the targets}}{V_0} = \frac{N 4\pi R^3}{3V_0} \tag{2.64}$$

and introducing the concentration of beads $c = \frac{N}{V}$ and the variable r we have for the probability

$$P_1(r) = \frac{4\pi}{3} c R_0^3 r^3. \tag{2.65}$$

During phagocytosis after cup formation the membrane needs to cover half of the spherical bead to run the second stage of engulfment. It appears from [41] (cited in [29]) that cup sizes are distributed mainly around half cup and full engulfment. We consider half engulfment position as critical to complete engulfment, we assume that when the cup get to half engulfment the macrophage is able to complete the process. We see the energy required to get halfway as a barrier of energy to cross. We have the energy $dE(\theta)$ for the phagocytic cup for each increment using eq.2.2.1:

$$dE(\theta) = 2\kappa 2\pi R^2 \left(\frac{R + R_0}{R}\right)^2 \sin(\theta) d\theta, \tag{2.66}$$

we integrate the spherical coordinate θ between 0 and $\frac{\pi}{2}$ to obtain the ΔE required to get cover half engulfment given by

$$\Delta E = 4\pi\kappa(1+r)^2. \tag{2.67}$$

We have introduced the nondimensional variable $\frac{R}{R_0}$ and κ is the bending modulus. The probability in terms of Boltzmann distribution to cross the energy barrier is guven by

$$P_2 \propto e^{-\beta\Delta E} \propto e^{-\beta\kappa 4\pi(1+r)^2}, \tag{2.68}$$

we introduce $\mu = 4\pi\beta\kappa$ and give the total probability combining the two events: the contact between the macrophage with a target and the barrier of energy to form a cup covering half of the bead. The product of the two probabilities is given by(see fig.2.15)

$$P(r) \propto \frac{4\pi N P_0 R_0^3}{3V_0} r^3 e^{-\mu(1+r)^2}. \tag{2.69}$$

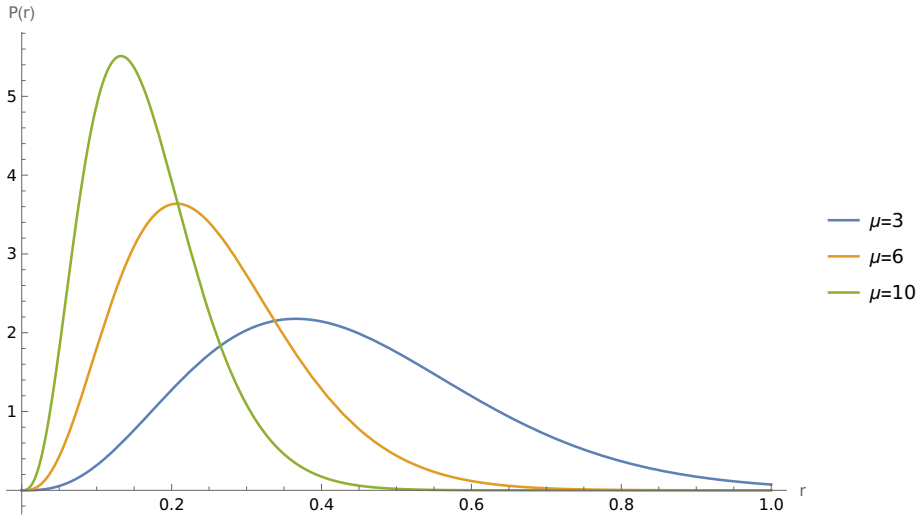

Figure 2.15: Probability distribution for different values of μ.

There is a maximum in this model in terms of a statistical event and not in terms of a single event. We differentiate eq.2.69 with respect to r given by

$$\frac{\partial P}{\partial r} = \frac{4\pi N P_0 R_0^3}{3V_0} e^{-\mu(1+r)^2} \left(3r^2 - 2\mu r^3(1+r)\right) = 0. \tag{2.70}$$

This leads to solving the polynomial in eq.2.71

$$-2\mu r^2 - 2\mu r + 3 = 0, \tag{2.71}$$

the solution for r^* is given by eq.2.72

$$r^* = \frac{2\mu \pm \sqrt{4\mu^2 + 24\mu}}{-4\mu}, \tag{2.72}$$

by simplifying we obtain $r^*(\mu)$ given by

$$r^*(\mu) = \frac{1}{2}\left(\sqrt{1 + \frac{6}{\mu}} - 1\right). \tag{2.73}$$

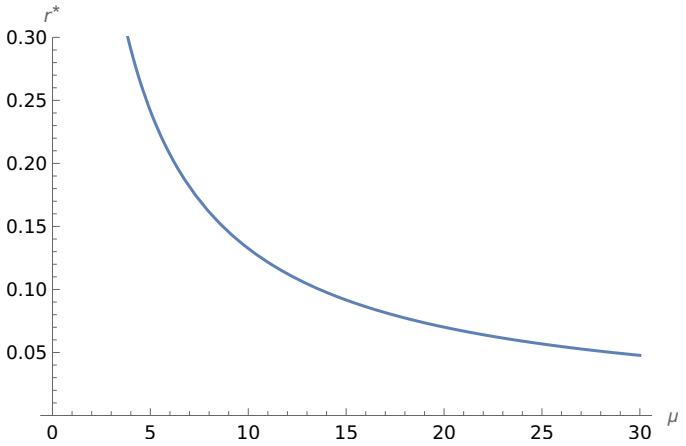

Figure 2.16: Plot describing how the location of the peak changes with μ

From experiments (table 1.1) we estimate r^*. We have also $\mu(r^*)$ using eq.2.72

$$\mu(r^*) = \frac{6}{4(r^* + \frac{1}{2})^2 - 1}. \tag{2.74}$$

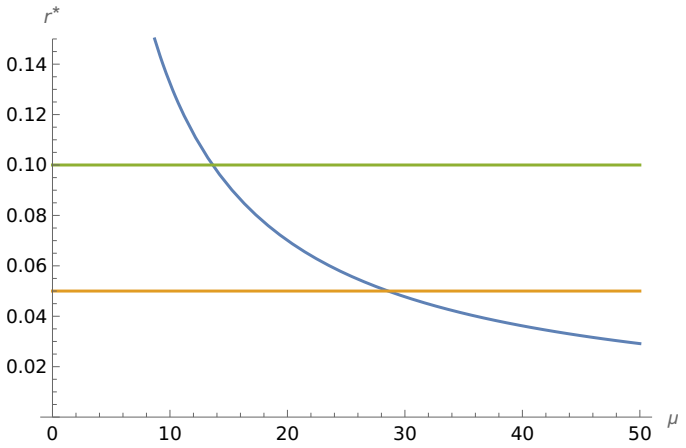

Figure 2.17: Location of the peak $r^*(\mu)$ and two lines showing the range of r^* based on estimation from table 1.1.

Since we have the location of the peak from previous experiments [36][6] shown in fig.2.17 it is possible to estimate the value of μ. We have the estimated range for the peak given by

$$0.05 < r < 0.1, \tag{2.75}$$

we estimate the corresponding value of μ around 15. This leads to the estimate for κ given by

$$\boxed{\kappa \approx k_b T}. \tag{2.76}$$

In practice the literature shows values of κ of about ten $k_b T$. Our estimate showing a less rigid membrane maybe explained by the fact that we are not considering the energy and/or adhesion or even actin helping to reduce the energy needed to fuel the process. This would allow the possibility of a more rigid membrane closer to values from the literature. The requirement for a softer membrane may indicate that the thermal fluctuations are not enough to have a realistic probability to engulf the target. Phagocytosis take up process requires active forces from actin and adhesion helping the membrane to reshape. Relying only on thermal fluctuation does not appear sufficient. With extra energy we could expect a stiffer membrane in our situation. It is an argument that take up processes are active and the case of an inert cell is very unlikely to lead to a take up.

2.6 Considering an extra source of energy

In this section the goal is to implement another source of energy that helps during the reshaping of the cell membrane. We consider a general energy per unit of surface form (see eq.2.77). This from has been used for adhesion to

study the energy profile of the nanoparticle wrapping [2] but in theory it could be the formulation of any other source of force in practice like from actin filament polymerisation. We will first see the new total energy of the system and secondly study the new probability to discuss the results

$$E_a = -UA, \tag{2.77}$$

U corresponds to an energy per surface area and A the area covered introduced by eq.2.77. Since it has the same form as surface tension $E_{tension} = \gamma A$ we can see also U as an effective energy per surface area $U_{eff} = \gamma - U$. In the case of our spherical bead the halfway engulfment by a phagocytic cup would give

$$E_a(2\pi R^2) = -2\pi U R^2. \tag{2.78}$$

Using $r = \frac{R}{R_0}$ we rewrite eq.2.78 into

$$E_a(r) = -2\pi U R_0^2 r^2, \tag{2.79}$$

we now have a formulation for the energy helping for membrane reshaping. The total energy $E = \Delta E + E_a$ and the expression is given by

$$E = E_a + 4\pi\kappa(1+r)^2 = 4\pi\kappa(1+r)^2 - 2\pi U R_0^2 r^2. \tag{2.80}$$

Adding the adhesion may give a threshold for U to be have a chance to engulf the bead. We have the new non-dimensional parameter f defined by

$$f = \frac{U R_0^2}{\kappa}, \tag{2.81}$$

we rewrite eq.2.80 with f in

$$E = 4\pi\kappa\left((1+r)^2 - \frac{f}{2}r^2\right) \tag{2.82}$$

and

$$\left(1 - \frac{f}{2}\right) r^2 + 2r + 1 > 0. \tag{2.83}$$

When this energy is negative the adhesion is sufficient to balance the curvature energy and consequently the shape fitting the bead. It brings a second parameter to determine. We are interested in the case where $E > 0$ (condition given by eq.2.83) in order to estimate the probability associated. It leads to a condition on f knowing that $0 < r < 1$. The polynomial is zero for the value of r given by

$$r_\pm = \frac{\pm\sqrt{2f} - 2}{2(1 - \frac{f}{2})}. \tag{2.84}$$

Considering $f > 0$ and $0 < r < 1$ we exclude r_+ to keep r_- giving positive values of r

$$r_- = \frac{2 + \sqrt{2f}}{2(\frac{f}{2} - 1)}. \tag{2.85}$$

We know from eq.2.85 the value of r for which eq.2.83 is zero. Since we consider $r < 1$ we can deduce for which value of f we have $r_- = 1$ using eq.2.85

$$\sqrt{2f} + 4 = f, \tag{2.86}$$

the solution of this equality is given by $f = 8$. We have two cases:

- $f < 8$: All the values for $0 < r < 1$ lead to a positive value of the energy. The total energy given by eq.2.82 acts as a barrier of energy. We can express the probability associated to the crossing of this barrier, since adhesion is not sufficient to balance bending, with thermal contribution to the process can help.
- $f > 8$: An interesting case is when a solution is for in the range $0 < r < 1$ because we can have both a positive and negative energy. As we increase f above 8 we end up having values of $r > r_-$ for which the energy in eq.2.82 is negative. Which means that we expect an engulfment since E_a in eq.2.79 is greater than the energy to form the cup given by eq.2.67, the energy barrier is not present anymore with a total energy being negative. For values of $r < r_-$ the energy barrier is positive and we have a similar situation to $f < 8$.

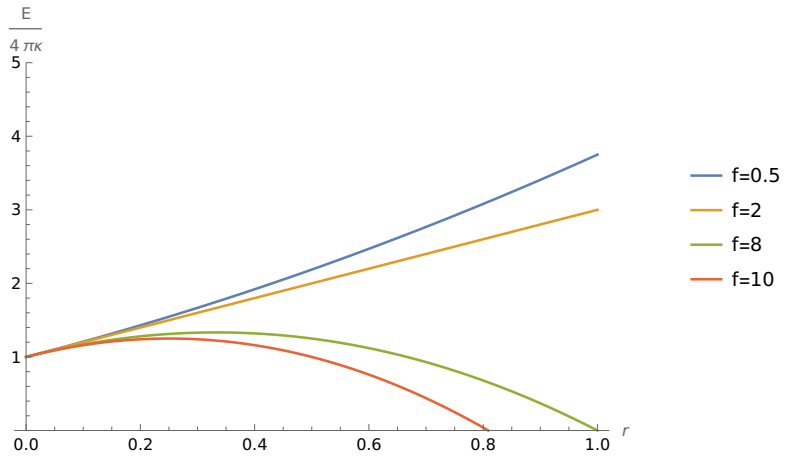

Figure 2.18: Energy from eq.2.82 in units of $4\pi\kappa$ for $0 < r < 1$. We notice for $f > 8$ the negative energy possible for $r > r_-$.

We have the probability associated to the energy in eq.2.82

$$P_f \propto r^3 e^{-\mu\left((1+r)^2 - \frac{f}{2}r^2\right)}, \tag{2.87}$$

we use the derivative $\frac{dP_f}{dr}$ to find the maximum of probability

$$\frac{dP_f}{dr} = -\mu r^3(2(1+r) - fr)e^{-\mu\left((1+r)^2 - \frac{f}{2}r^2\right)} + 3r^2 e^{-\mu\left((1+r)^2 - \frac{f}{2}r^2\right)} = 0, \tag{2.88}$$

since we take $r \neq 0$ we consider the solution for which

$$(f - 2\mu)r^2 - 2\mu r + 3 = 0. \tag{2.89}$$

The solution is given by

$$r_{\pm} = \frac{2\mu \pm \sqrt{4\mu^2 - 12(f - 2\mu)}}{2(f - 2\mu)}. \tag{2.90}$$

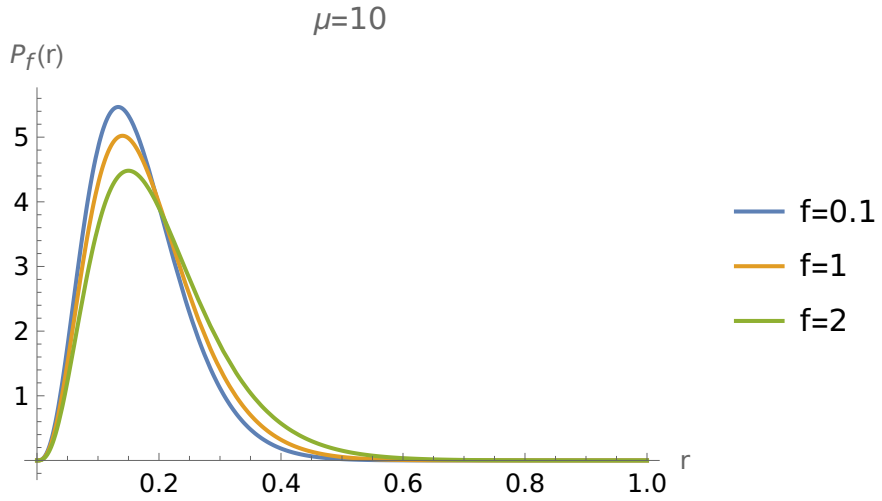

Figure 2.19: Probability $P_f(r)$ for different values of f.

Writing the solution from eq.2.90 in a simpler form verifying that when $f = 0$ we recover the result given by eq.2.73 (see fig.2.20)

$$r^*(\mu, f) = \frac{1 \pm \sqrt{1 - \frac{6}{\mu}(\frac{f}{2\mu} - 1)}}{2(\frac{f}{2\mu} - 1)}, \tag{2.91}$$

we notice a condition on μ to have a positive term in the square root which leads to the inequality

$$1 - \frac{6}{\mu}\left(\frac{f}{2\mu} - 1\right) > 0. \tag{2.92}$$

The condition turns out to be a minimum value for μ as shown in

$$\mu > 3\left(\sqrt{1 + \frac{f}{3}} - 1\right). \tag{2.93}$$

For $f = 0$, μ has to be larger than μ_{min} to consider a probability any value of $\mu < \mu_{min}$ will have an adhesion high enough to engulf the bead.

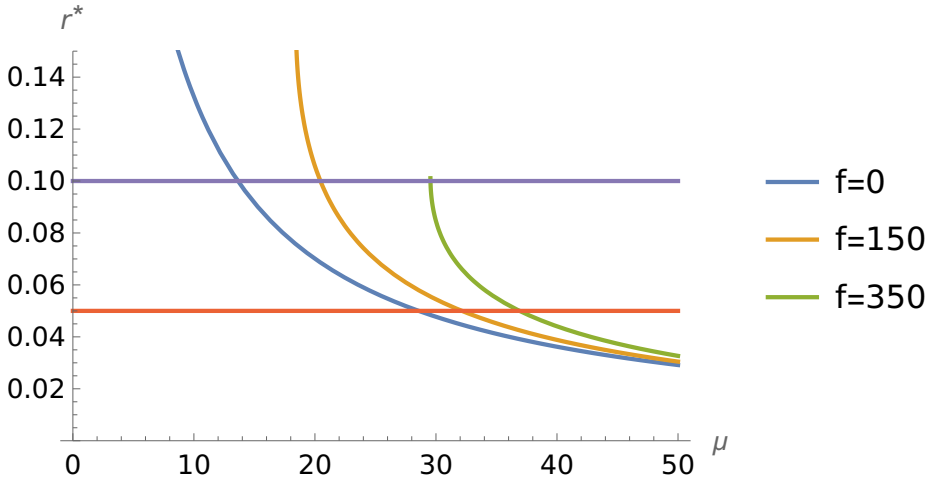

Figure 2.20: Location of the optimum size r^* with μ for different values of f.

From the result in fig.2.20 we can comment on the value of $f(r)$ and $\mu(r)$. From there we see that for the same location of the maximum of probability we can expect a higher value of μ for a higher f. It means that physically we can allow a stiffer membrane for the same $r*$ in the case with f since it is reducing the total energy of the system.

2.6.1 Surface tension case

We take the crossover length given in [2] as

$$l_{crossover} = \sqrt{\frac{\kappa}{\gamma}}, \tag{2.94}$$

to estimate the lengthscale for which surface tension energy dominates. The estimation given by [2] is about 100 to 200 nm where surface tension is taken from [33]. We want to study this possibility where surface tension dominates and can be written

$$E_{eff} = (\gamma - U)A = U_{eff}A \tag{2.95}$$

We write down the probability using eq.2.95

$$P_{eff} \propto r^3 e^{-2\pi R_0^2 \beta U_{eff} r^2}, \tag{2.96}$$

the derivative equal to zero gives

$$\frac{dP_{eff}}{dr} = 3r^2 - 4r\pi R_0^2 \beta U_{eff} r^3 = 0. \tag{2.97}$$

The solution for r is given by

$$r^*_{eff} = \sqrt{\frac{3}{4\pi R_0^2 \beta U_{eff}}}. \tag{2.98}$$

Knowing from table 1.1 that we expect $R_eff = r^*_{eff} R_0$ to be around $0.5\mu m$ we estimate U_eff

$$U_{eff} = \frac{3}{4\pi\beta R^{*2}_{eff}} \approx 10^{-6} J/m^2, \tag{2.99}$$

this estimate is close to the values of surface tension γ, used in [2] to estimate eq.2.94.

2.6.2 Pseudopod energy

Another possible way to describe the energy is to take the energy term of related to the pseudopods engulfing the target instead of the cup from eq.2.24 keeping the term $2\pi^2\kappa\frac{R}{e}$ that we can write as

$$P_{pseudo} = P_1 P_e \propto r^3 e^{-\beta(2\pi^2\kappa\frac{R_0}{e}r)} \tag{2.100}$$

Differentiating eq.2.100 we have eq.2.101.

$$3r^2 - 2\pi^2\beta\kappa\frac{R_0}{e}r^4 = 0 \tag{2.101}$$

Ignoring the solution $r = 0$ we have the solution given by eq.2.102.

$$r^* = \frac{3}{2\pi^2\beta R_0\sqrt{2\gamma\kappa}} \tag{2.102}$$

The size $R = \frac{3k_bT}{2\pi^2\sqrt{2\gamma\kappa}}$ can be estimated by taking values of γ and κ used by [2] and taken from [33]. We find $R \approx 10^{-7}m$ and is in the range of values given in table.1.1.

2.7 Target orientation

The target is considered being a closed surface with an average curvature describing the local shape at different points of the surface. The local curvature seems to be an important factor to determine the capacity of the cell to complete the take up of the target. We suppose that the target is oriented in a random way at the point of contact with the cell. Knowing the shape one can estimate the probability to encounter a given curvature H at that point. The simplest case is the sphere since the curvature is the same on the entire surface of the target $P_H = 1$. A more interesting case is the spherocylinder where we have two possible curvature $H_{Sphere} = \frac{1}{R}$ and $H_{Cylinder} = \frac{1}{2R}$. The two probabilities (see fig.2.21) associated are given by eq.2.105 and eq.2.106 defined by

$$P_{Sphere} = \frac{S_{Sphere}}{S_{Total}} \tag{2.103}$$

and

$$P_{Cylinder} = \frac{S_{Cylinder}}{S_{Total}}. \tag{2.104}$$

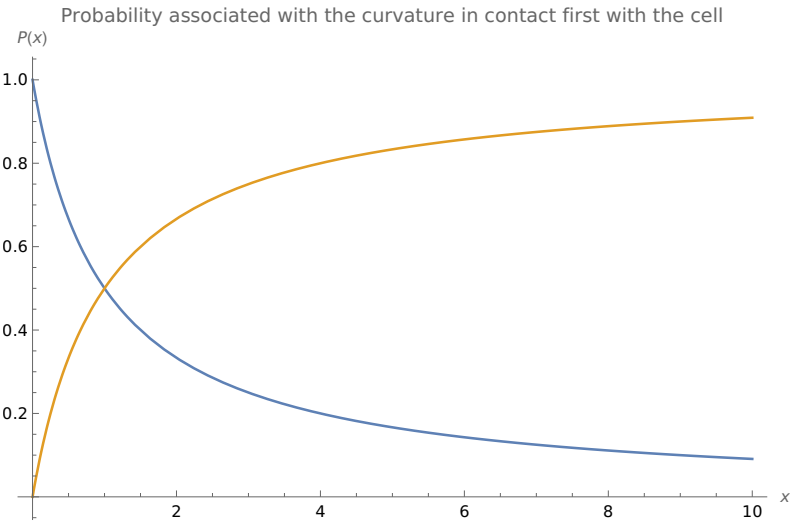

Figure 2.21: Probability associated to the curvature that can randomly be in contact with the cell. It shows how the shape changes the curvature a macrophage may encounter when finding a target. It has an impact on the probability of engulfment.

Replacing with the surface of the sphere and cylinder we obtain

$$P_{Sphere} = \frac{4\pi R^2}{4\pi R^2 + 2\pi RL} = \frac{1}{1 + \frac{L}{2R}} \tag{2.105}$$

and

$$P_{Cylinder} = \frac{2\pi RL}{4\pi R^2 + 2\pi RL} = \frac{1}{1 + \frac{2R}{L}}. \tag{2.106}$$

Introducing $x = \frac{2R}{L}$ we have

$$P_{Cylinder}(x) = \frac{1}{1+x} \tag{2.107}$$

and

$$P_{Sphere}(x) = \frac{1}{1 + \frac{1}{x}}. \tag{2.108}$$

2.8 Discussion

Taking the previous results we now open the discussion by comparing with results from the literature. We start first by commenting on the existence of a peak in bead intake by a macrophage. The general approach of considering the Helfrich energy with its bending term in particular involving curvature. It

appears that no sphere radius $R \neq 0$ minimises the energy. We have next considered the wrapping of a spherocylinder finding a way to minimise the bending energy with a relationship between the cylinder length and hemispheres radius.

As the results from table 1.1 were performed with spheres we investigated another model in section 2.4. The result obtained shows a coupling between cortex thickness and range of the interaction representing the repulsion from volume exclusion. If we take a range for R the optimum size from table 1.1 and cortex thickness from [5] we can give an estimate using eq.2.51

$$\gamma = 2\left(\frac{2R}{e} + 1\right), \tag{2.109}$$

taking $R = 0.5\mu m$ and $e = 0.350\mu m$ in eq.2.109 the value of $\gamma \approx 7.7$. The value of γ is sensitive to the estimate e. The determination of cortex thickness seems to be challenging partly due to light scattering at that scale and the active specificity of the cortex which means that the thickness can change depending on the situation if more force is required for example especially in actin dependant processes like phagocytosis and macropinocytosis. A last remark is that even if we calculated a radius size we could also interpret it as an optimum curvature for a sphere.

Another aspect we highlighted in section 2.5 is the the probability of contact. In fact the results obtained in the experiments (see table1.1) consider in practice a population of macrophages and beads. Before getting to the intake process the cell has to be in contact with a bead which itself is not guaranteed which leads us to see it as a probability of contact. This probability is combined then with a probability to take the engulfment cup at half of the process. We found a value of for the bending modulus with a lower value compared to the literature but with the addition of an energy per unit of surface it allows to increase the bending modulus value bringing it closer to estimated values in the literature (used to estimate eq.2.22). This indicates the necessity of an energy to run the engulfment.

2.9 Summary

As a conclusion we summarise the work done in this chapter. We first used Helfrich formulation energy to quantify the energy associated with a deformed curved surface for a sphere and spherocylinder. The sphere case has not been able to reproduce the observed preferred size suggested by works from the literature. So we looked for other approaches aiming to find a model that could explain the observations. The second model introduces a simple model for the cortex with an excluded volume effect that highlights the role of thickness cortex with interactions in an optimum of energy. We concluded the chapter with a last model combining probability for the macrophage to make contact with a bead with the probability of reaching half engulfment showing a higher intake for a particular bead size.

Chapter 3

Phagocytosis: Dynamical aspects of engulfment

This part is oriented towards the time evolution of engulfment. The aim is to propose a model describing the potential mechanisms behind cup growth around a spherical bead during the take up. To interpret and quantify the observation (see [29][28]) we take a parameter that is suited to indicate the progression. It is mostly the length around the bead that the membrane is running through. A simple parameter in the case of a spherical object is the angle $\theta_c(t)$ from spherical coordinates that can be used to simplify the parametrisation of the problem. Their analysis of the observation with video tracking of the engulfment can be found in [29][28]. From this starting point we take the different phases during the progression represented in fig.3.1 and focus on the fastest phase before the closure of the cup. If phase II is modelled as a diffusive process, that we explain in section 3.1, the next phase requires an addition of a term to the equation to observe a faster progression. The model we propose does not involve the presence of any diffusion of receptor or signalling molecules (reviewed in [28]) on the surface of the membrane but is a fluid model not involving signalling. Since our model is not involving the surface of the target it will be interesting to discuss it in the context of macropinocytosis.

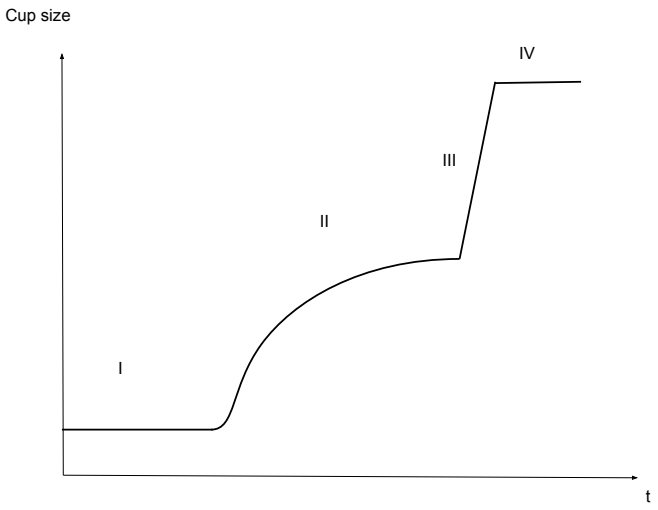

Figure 3.1: Schematic representation of the different steps in the phagocytosis taken from [28][29]. In our work we focus on the step III by giving a possible mechanism to explain it.

3.1 The challenge of modelling engulfment

Engulfment performed by a cell or macrophages specialised in endocytosis after being observed has been at the centre of models aiming to explain the mechanisms behind to predict the outcome of an engulfment given the parameters of the problem like size and shape of the target. The model given by [12] uses diffusive model receptors with ligands on the surface of the membrane on one side and the target on the other, to give a time evolution of the phagocytic cup progression. Sizes studied go up to few hundreds of nanometres and highlights the optimal size to obtain the lowest engulfment time. The model does not require the implication of the cortex on the contrary of the more recent work from [39] that describes the engulfment of the membrane using actin ratcheting and ligand-receptor adhesion. In the last case it appears that the actin concentration is not sensitive to the size of the bead. The numerical model in 2d given in [4] implementing actin filaments,bending and membrane tension investigates the engulfment time for different bead sizes. Despite a possible optimal size for time engulfment more work would be required for more statistical relevance. We note also that what is meant by optimal size can refer to time optimisation or the number of beads per cell when the experiment is performed on a large group of cells and beads. The parallel of an optimum size that would be the same for both cases does not seem obvious to us and it would be more cautious to distinguish time optimisation and higher rate of endocytosis when counting

on a large group of cells experiment.

3.2 Feedback model

In the following sections we introduce our model offering a possible explanation for the observation made above. The different steps require fluid mechanics and pressure forces we introduce the fig.3.2 and 3.3 to visualise the feedback and describe each one after.

The process requires few assumptions to start:

1. The phagocytic cup is formed.
2. The target has a spherical shape.
3. The cell has engulfed at least half of the sphere.

The process requires a flow surrounding the upper part of the spherical target. The flow is supposed to carry actomyosin or actin alone generating the force required to engage the process. In order to observe a flow we need a spatial gradient of pressure.

The pressure difference needed comes from the difference between the bottom of the sphere where the phagocytic cup holds the bead in place and the upper part where the fluid is progressing. The flow is assumed to carry more actin on top of the target creating a difference of pressure due to the force exerted. Since we neglect elastic forces of the membrane, we are in a case of a small bead under few 100 nm for which above surface tension may become more significant (see [2]). Once the pressure difference is established with the flow going around the target the feedback becomes possible. To explore this loop we describe each step. From the pressure description to the fluid flow. For the next sections we define $\theta_c(t)$ as the progress of the engulfment so that $\theta_c(t=0) = \frac{\pi}{2}$ which is the starting point of the second stage for a sphere.

3.2.1 Pressure

In this section we calculate the expression of the pressure from the bead on the fluid on the bottom. We remind the element of surface for a sphere with R_b the radius of the bead

$$dA = R_b^2 sin(\theta) d\theta d\phi, \tag{3.1}$$

the force from the actin pushing on the surface generated by actin filament polymerisation with a component of the force normal to the surface on dA. The total force is the sum in eq.3.2 of all the elements i

$$\vec{F} = \sum_i \vec{f}_i. \tag{3.2}$$

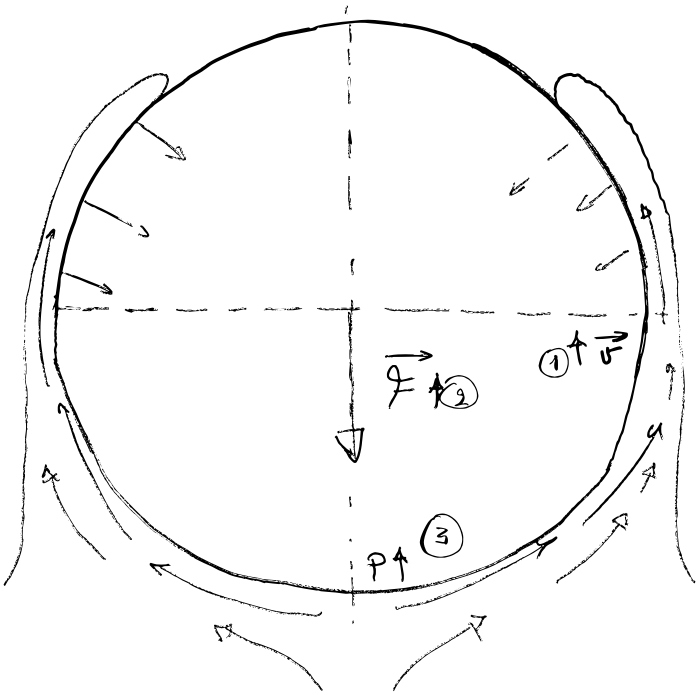

Figure 3.2: Schematic representation of the process. The element 1 represents the fluid flow speed. The element 2 the force exerted toward the cell and element 3 shows the increase of pressure P.

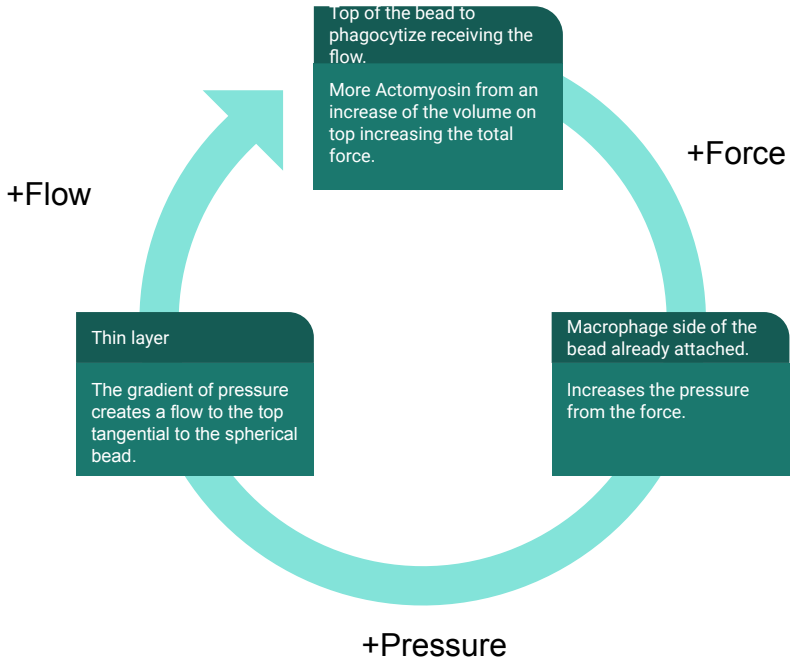

Figure 3.3: Feedback loop representation.

The continuous form of the force can be written with the introduction of $\rho_{actin}(\vec{r})$ the density of actin covering the membrane on the surface of the bead

$$F = f_i \int dA(\vec{r})\rho(\vec{r}), \tag{3.3}$$

we supposed the force of each filaments producing the same normal force to the surface. If the density of actin is homogeneous on the surface the equation can be simplified with S the surface considered and ρ_{actin} the density of actin on S

$$F = f_i \rho_{actin} S. \tag{3.4}$$

The radial pressure is given by

$$P_0 = f_i \rho_{actin} \tag{3.5}$$

and the total force produced given in eq.3.6 following the z-axis can be given by multiplying by the surface increasingly covering the upper part of the bead. This means that the more the engulfment is progressing the higher the force from the bead on the fluid will increase. The projection on the z-axis of this pressure on the fluid of the macrophage gives

$$F_z = \pi R^2 P_0 \cos\theta_c. \tag{3.6}$$

On another hand we keep the radial component with the surface on the lower part $0 < \theta < \frac{\pi}{2}$. Leading to

$$F = \pi R^2 P_0 \cos\theta_c \cos\theta, \tag{3.7}$$

dividing by the element of surface we finally obtain the pressure on the bottom of the bead as a function of the variables (θ_c, θ), θ_c being the angle of the cup progression and θ the spherical coordinates parameter

$$\boxed{P(\theta_c, \theta) = -P_0 \cos(\theta_c(t)) \cos\theta}. \tag{3.8}$$

3.2.2 Fluid flow

The difference of pressure coming from P has to be linked with the flux going around the bead. We can expect in general that the flux or the speed going from the bottom side to the upper side of the bead is a function of the difference of pressure ΔP and viscosity of the fluid μ.

With a non zero flow going to the top of the bead the angle θ_c will be increasing. Since we consider an incompressible fluid we can relate the flux of volume to the increase angle. We first write down the flux Q that goes from bottom to top of the bead through the cross sectional area S at $\theta = \frac{\pi}{2}$ in eq.3.9 introducing v the speed of the flow through the section S

$$\vec{Q} = S\vec{v}, \tag{3.9}$$

the surface S corresponds to the macrophage protrusion located halfway ($\theta = \frac{\pi}{2}$) of the bead. We have in eq.3.10 the expression of the surface at that point with ϵ the thickness of the cup leading the engulfment around the bead

$$S = \pi \left((R_b + \epsilon)^2 - R_b^2 \right) = \pi \left(\epsilon^2 + 2\epsilon R_B \right). \tag{3.10}$$

Combining eq.3.9 and eq.3.10 we can deduce

$$Q = 2\pi v \epsilon R_b \left(1 + \frac{\epsilon}{2R_b} \right), \tag{3.11}$$

in the case where $R_b >> \epsilon$ eq.3.11 can be simplified to

$$Q = 2\pi v \epsilon R_b. \tag{3.12}$$

We introduce the element of volume dV added by the flux Q given by

$$dV = 2\pi R_b^2 \epsilon sin(\theta_c) d\theta_c \tag{3.13}$$

and integrate $d\phi$ and dr keeping $d\theta_c$ to express dV with θ_c in spherical coordinate

$$dV = 2\pi d\theta_c \sin(\theta_c) \left[\frac{r^3}{3} \right]_{R_b}^{R_b+\epsilon}. \tag{3.14}$$

We divide by dt eq.3.13 to obtain

$$\frac{dV}{dt} = Q = 2\pi R_b^2 \epsilon sin(\theta_c) \theta_c'(t) \tag{3.15}$$

and by establishing the equality between 3.12 and 3.15 we have

$$2\pi R_b^2 \epsilon \sin(\theta_c) \theta_c'(t) = 2\pi v \epsilon R_b, \tag{3.16}$$

This finally leads to the following differential equation in

$$\boxed{\theta_c'(t) = \frac{v(\theta_c(t))}{R_b \sin(\theta_c(t))}}. \tag{3.17}$$

3.3 Solutions

In the following section we propose possible solutions by establishing the expression of $v(\theta_c(t))$. To find this expression we have to choose a model for the fluid dynamics. We start with Darcy's law that includes porosity and finally an approximation based on Stokes flow neglecting inertial forces.

Case 1: Darcy's law

We introduce Darcy's law, describing a viscous flow through a porous environment, expression in eq.3.18. k is the permeability of the media and η the dynamical viscosity

$$\vec{q} = -\frac{k}{\eta}\vec{\nabla}P(\theta), \tag{3.18}$$

with q the speed of the flow. We use the expression of eq.3.8 to calculate the gradient of pressure in

$$\vec{\nabla}P = \frac{P_0}{R_b}\sin\theta\cos\theta_c\vec{e_\theta}, \tag{3.19}$$

we deduce from eq.3.18 and eq.3.19 the equation on the flow

$$\vec{q} = -\frac{kP_0}{\eta R_b}\sin\theta\cos\theta_c\vec{e_\theta}. \tag{3.20}$$

We are interested in a steady state flow localised around $\theta = \frac{\pi}{2}$. We end up with differential equation

$$\tan\theta_c\theta_c' = -\frac{kP_0}{\eta R_b^2}, \tag{3.21}$$

we identify the parameter $\tau = \frac{\eta R_b^2}{kP_0}$ the characteristic time of the process. We write eq.3.21 in a simpler form with

$$\tan\theta_c\theta_c' = -\frac{1}{\tau}. \tag{3.22}$$

The characteristic time is defined as

$$\tau = \frac{\eta R_b^2}{kP_0}. \tag{3.23}$$

The integration of eq.3.22 gives the solution using the initial time as $t = 0$ and $\theta(0) = \theta_0$ the initial condition

$$\ln\frac{\cos\theta_0}{\cos\theta_c} = -\frac{t}{\tau}. \tag{3.24}$$

To have a solution we need to consider $\theta_0 > \frac{\pi}{2}$. The expression of $\theta_c(t)$ is finally given by eq.3.25 (see fig.3.4)

$$\theta_c(t) = \arccos\left(\cos\theta_0 e^{\frac{t}{\tau}}\right). \tag{3.25}$$

We deduce from the solution that the duration of the last part of the phagocytosis which means the phase III to close the cup is t^* given in eq.3.26 and represented in fig.3.5

$$t^* = -\tau\ln(-\cos\theta_0). \tag{3.26}$$

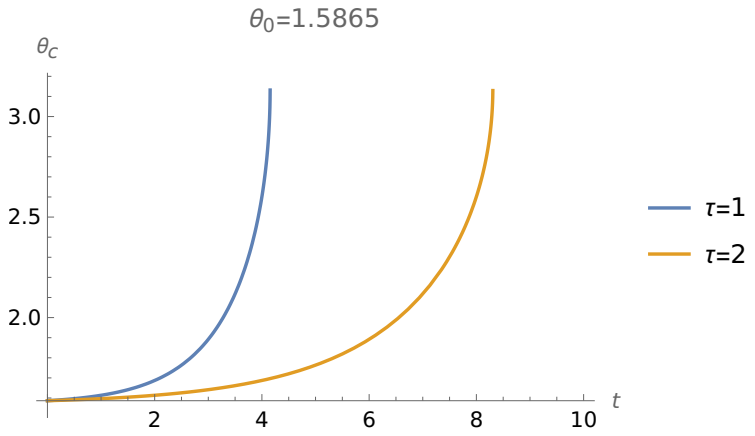

Figure 3.4: Evolution of engulfment of the upper side of the bead through $\theta_c(t)$, that goes from $\frac{\pi}{2}$ to π i our case. We show the evolution for different values of τ.

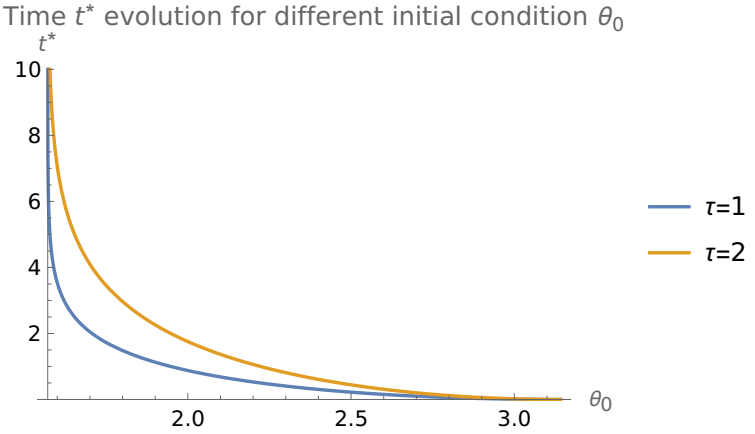

Figure 3.5: Effect of the initial condition $\theta_c(0) = \theta_0$ for different τ.

Case 2: Stokes flow

Taking the creeping flow around a sphere commonly called Stokes flow given by eq.3.27. The equation is valid considering we neglect inertial forces in a situation of low Reynolds number ($Re << 1$) [34]

$$F = 6\pi\eta R_b v. \tag{3.27}$$

- F corresponds to the force pushing our bead.
- R_b the radius of the sphere.
- η is the viscosity of the fluid.
- v is the speed of the flow around the sphere.

We take the expression of the speed v using eq.3.27

$$v = \frac{F}{6\pi\eta R_b}, \tag{3.28}$$

we take the maximum of pressure at the bottom which corresponds to $\theta = 0$. The force is expressed by

$$F = \pi R_b^2 P_0 \cos\theta_c(t). \tag{3.29}$$

Replacing eq.3.29 in eq.3.28 we have the expression of v given by

$$v = \frac{\pi R_b^2 P_0 \cos\theta_c(t)}{6\pi\eta R_b} = \frac{P_0 R_b \cos\theta_c(t)}{6\eta}, \tag{3.30}$$

the differential equation is

$$\sin(\theta_c)\theta_c'(t) = \frac{P_0}{6\eta}\cos\theta_c. \tag{3.31}$$

We end up with eq.3.22 as the same equation to solve with τ given by eq.3.22. In that case the τ has a different expression compared to the case with porosity

$$\tau = \frac{6\eta}{P_0}. \tag{3.32}$$

3.4 Estimation of the characteristic time τ

Energy fluctuation corresponding to the smallest increment of $d\theta$ for $\theta = \frac{\pi}{2}$ from the bending term in Helfrich energy in eq.2.2 for the phagocytic cup gives

$$d\theta = \frac{dE}{4\pi\kappa(1+r)^2}, \tag{3.33}$$

for a thermal fluctuation we replace dE by kT

$$d\theta = \frac{kT}{4\pi\kappa(1+r)^2}. \tag{3.34}$$

We end up with the following θ_0 as an initial condition for the angle

$$\theta_0 = \frac{\pi}{2} + d\theta, \tag{3.35}$$

we can write the cosine of eq.3.35

$$\cos\left(\frac{\pi}{2} + \frac{kT}{4\pi\kappa(1+r)^2}\right) = -\sin\frac{kT}{4\pi\kappa(1+r)^2}. \tag{3.36}$$

Replacing in eq.3.26 the expression in eq.3.36 gives

$$t^* = -\tau \ln\left(\sin\frac{kT}{4\pi\kappa(1+r)^2}\right). \tag{3.37}$$

We can write a simpler form assuming that κ is large compared to kT (see Chapter 2). We expand $\sin x \approx x$ and $(1+r)^2 \approx 1$ meaning that the bead size is small compared to the macrophages. We end up with

$$\boxed{t^* = \tau \ln\frac{4\pi\kappa}{kT}}, \tag{3.38}$$

condition $4\pi\kappa >> kT$ must be true in order to keep the approximation of the sine valid. We use the ratio $\frac{4\pi\kappa}{kT}$ as μ and have $\frac{t}{\tau}$ describing how the factor $\ln\mu$ can change the time of engulfment.

The characteristic time of engulfment is multiplied by the logarithmic factor in eq.3.38. Taking $\kappa \approx 10kT$ gives a value of $\mu \approx 100$. The logarithm increases slowly despite the large values of μ. In the case where $\mu \approx 100$ we have $ln(100) \approx 4.6$. The evolution of $\frac{t^*}{\tau}$ with μ is dumped by the logarithm function. We see a large increase until $\mu \approx 50$ and a slowly increasing time with μ (see fig.3.6)

$$t^*(\mu = 100) \approx 4.6\tau. \tag{3.39}$$

To estimate τ one may need the value of the pressure P_0 applied by the actin on the surface with the viscosity μ and the permeability k in the case of Darcy's law.An actin filament is able to generate few piconewton in terms of force. To estimate the pressure that the cortex is able to produce we need the surface s on which this force is applied. We can consider a minimum surface s too in a very packed configuration where s tends to the thickness of the actin filament of around 7 nm [19].

We can give the following range for the smallest surface and the associated maximum pressure applied

$$s_{min} = 50nm^2 \tag{3.40}$$

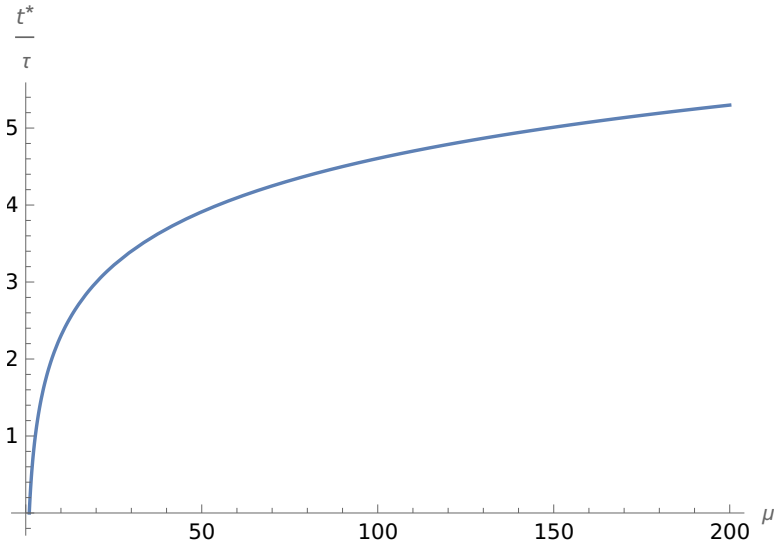

Figure 3.6: Evolution of time engulfment $t^*(\mu)$ for phase III in units of τ.

and

$$P_{max} = \frac{10^{-12}}{5.10^{-17}} = 20kPa. \tag{3.41}$$

We have now two values two values of τ to estimate. In practice phase III is estimated to last $t^* \approx 2s$. We can take this value and deduce in the case of Stokes flow with eq.3.32 an estimate of η. In addition to that we use eq.3.39 to estimate τ as $\tau = \frac{t^*}{4.6} \approx 0.4$

$$\eta = \frac{P_0\tau}{6} = \frac{20.10^3\tau}{6} \approx 10^3 Pa.s. \tag{3.42}$$

In the case of the time estimation using Darcy's law we propose an estimate of the permeability k based on the viscosity found in eq.3.42. Using eq.3.23 the permeability is estimated

$$k = \frac{\eta R_b^2}{\tau P_0} \approx \frac{10^3 10^{-12}}{2.20 * 10^3} \approx 10^{-14} m^2. \tag{3.43}$$

It suggests a pore size of 100 nm which is close to values mentioned in section 1.2.4.

3.5 Summary

In this section we have presented a model requiring only a feedback loop using fluid mechanics and requiring the participation of actin pushing from the top feeding the process in energy. This process does not require ligands or the

diffusion of a mobile receptor but does not exclude it also. Interestingly since not requiring receptor-ligand adhesion could be also used for pinocytosis where we have only the fluid to drink and so no adhesion is possible. After establishing the differential equation we used two different formulations to establish a relationship between pressure or force and the speed flow. The noticeable difference is the dependency with R_b the radius of the bead. Darcy's formulation with permeability parameter k is proportional to R_b^2 but using the Stokes flow relationship the time is independent from R_b. The time we estimated is only for phase III meaning that it concerns only the quick stage of engulfment of the last half of the bead.

Chapter 4

Nucleus: Deformation and constriction crossing

The following chapter aims to understand the conditions and mechanisms of cell crossing a narrow constriction, which can occur during cell migration. The nucleus being stiffer than the rest of the cell we take the nucleus as the limiting elastic element of the cell. This means that if the nucleus crosses the constriction the whole cell can cross. To perform successfully the crossing the nucleus needs a reshaping to fit in the tunnel after the entrance. An external force to the nucleus but internal to the cell. The force will exert a pressure on the back of the nucleus to get it through the smaller constriction and cross the channel. The pressure generated on the nucleus, or pressure, is not limited to any biological process but actin polymerisation is considered as a good candidate, therefore we will use the force generated by actin filament as a good candidate when approximating the value of the pressure. For experiments we refer to [37] and for numerical work to [10]. Our results will be compared with results from the literature and open the discussion on how a theoretical model combined with experiments could be useful for a better understanding of the cell structure and mechanisms that may be challenging to obtain experimentally. The first sections will focus on static friction at the entrance of the constriction and 2d models showing how a condition on crossing can be obtained. We will conclude with a model giving a probability of crossing that we compare with results from [37] and [35].

4.1 Nucleus through the channel

We introduce a model for the nucleus and consider the limitation to enter from the static friction between the nucleus membrane and its environment that we define as μ. We start from a state where the nucleus can move freely i.e. not bounded on the lateral sides, to a channel with a smaller section compared to the nucleus. The nucleus is considered having a spherical shape with the front side surface in contact with the constriction of radius a being

$$S = \pi \left(R_0^2 - a^2\right). \tag{4.1}$$

For the simplicity of the calculation we consider a circular constriction which means that the 3d structure is a cylinder. We use surface S for static friction force and pressure P to give the expression of the static force

$$F_f = -\mu_s P S. \tag{4.2}$$

On the other hand we have the force coming from the cell itself pushing inside the constriction on the nucleus coming from the cell itself, the force does not come from any external element, given by

$$F_a = PS_a = \pi a^2 P. \tag{4.3}$$

The sum of the two forces should be positive to expect a possible movement towards the constriction and overcome the static friction and is given by

$$F_a + F_f > 0. \tag{4.4}$$

This leads to the condition on a to allow the nucleus to move into the constriction given by

$$Pa^2\pi - \mu_s \pi P(R_0^2 - a^2) > 0. \tag{4.5}$$

Simplifying P as we consider that $P \neq 0$ we deduce a condition on the size of the entrance given by

$$\boxed{a > \sqrt{\frac{\mu_s}{1+\mu_s}} R_0}. \tag{4.6}$$

We introduce $\alpha = \frac{a}{R_0}$ to write eq.4.6 into (see fig.4.1)

$$\alpha > \sqrt{\frac{\mu_s}{1+\mu_s}}. \tag{4.7}$$

The static friction coefficient being rarely greater than 1 for most materials we can estimate a value of α that should be large enough for any material

$$\boxed{\alpha(\mu_s = 1) = \frac{1}{\sqrt{2}} \approx 0.7}. \tag{4.8}$$

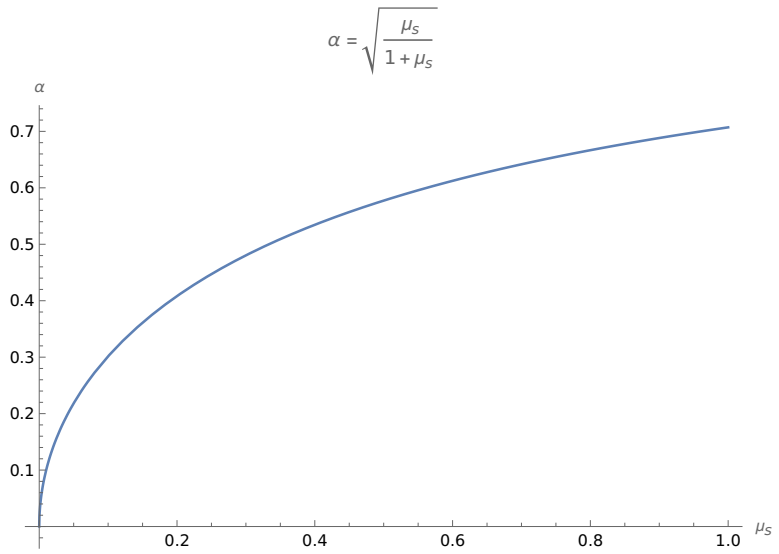

Figure 4.1: Evolution of α with the static friction coefficient μ_s.

The absence of the pressure P in the result of the condition to allow the movement of the nucleus toward the constriction does not ultimately mean that it is not relevant during the dynamics and inside the constriction. It is a necessary condition but not sufficient since that it does not take into account the tunnel after the constriction that we see in section 4.2. Knowing experimentally the minimum radius a_{min} required to start the movement through the constriction we can estimate the value of the static friction coefficient with fig.4.1

$$\mu_s = \frac{\alpha_{min}^2}{1-\alpha_{min}^2}. \tag{4.9}$$

It means that experimentally if we know the value of α_{min} for which the nucleus can move into the constriction we can deduce an estimated value of μ_s (see fig.4.2).

4.2 2d model of the nucleus for the elastic sheet

In this section we introduce a model to describe the progression of the nucleus in the channel (see fig.4.3).We consider a force from actomyosin applied on the back of the nucleus all along the segment in 2d (for a 3d model it will be a surface). The nucleus is described as a 2d shell structure with the nuclear envelop. This implies that instead of a 2d closed surface we have a 1d elastic rope representing the shell. To build the model we translate the different biological elements to forces and we simplify the shape of the undeformed nucleus to a square initially

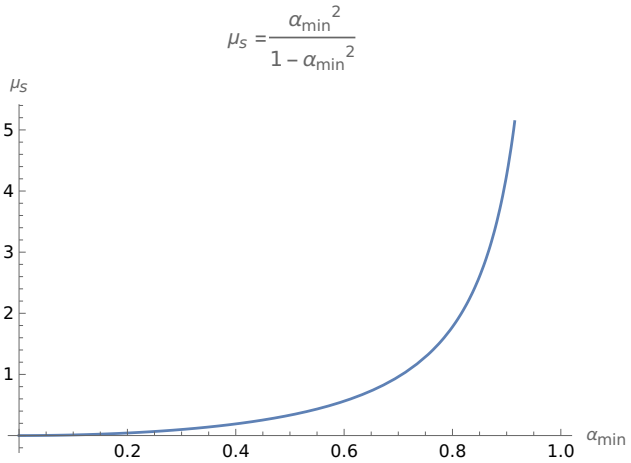

Figure 4.2: Value of μ_s with the minimum value of $\alpha = \alpha_{min}$ to observe a possible crossing.

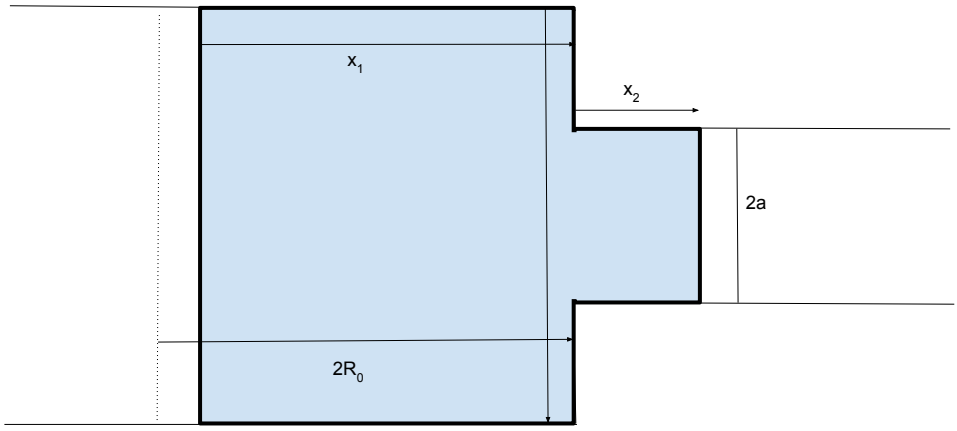

Figure 4.3: Drawing of the nucleus representation entering a constriction of size $2a$.

of size $2R_0$. We consider that during the process the nucleus follows the shape of the channel . We have two forces: a force resulting from the pressure, from the force generated by the actomyosin in the cell, pushing toward the entrance and an elastic resistance because the nucleus tends to keep its initial shape. The state of equilibrium of forces is reached when the following equation is true

$$\vec{F}_{elastic} + \vec{F}_{pressure} = \vec{0}. \tag{4.10}$$

The elastic force comes from the elasticity of the nucleus membrane We consider the membrane as an elastic rope with a negligible thickness compared to the nucleus radius. We use a 1d model shell to describe the elasticity of the envelope with k the elastic constant

$$F_{elastic} = -k(2x_1 + 2x_2 + 4R_0 - 8R_0). \tag{4.11}$$

The force pushing toward the constriction and deforming the nucleus comes from the actomyosin network pushing toward the entrance as shown in [37]. The total force at the back of the nucleus can be written in a discrete way by summing the contribution of each discrete element representing the actomyosin. These mathematical elements are not strictly limited to any specific molecule or filament

$$F_{actin} = \Sigma_i \vec{f}_i. \tag{4.12}$$

From the expression of the force we get the expression of the pressure P

$$P = \frac{F}{S}. \tag{4.13}$$

In the 2d case the element of surface becomes an element of length $\vec{dS} \to \vec{dl}$. The force f_i corresponds to the single element of force and we introduce n_{actin} as a linear density. The discrete sum can be replaced by

$$P = f_i n_{actin}. \tag{4.14}$$

We suppose the pressure pushing to the entrance as uniform. The equilibrium of forces gives us

$$2Pa - k(2x_1 + 2x_2 + 4R_0 - 8R_0) = 0. \tag{4.15}$$

We assume that the nucleus is incompressible, which means that the total volume is constant when reshaping [10], this leads us to say that the surface in 2d remains constant $A = 4R_0^2$. This allows us to establish a relationship between x_1 and x_2 with

$$4R_0^2 = 2R_0 x_1 + 2a x_2, \tag{4.16}$$

which leads to an expression x_1

$$x_1 = 2R_0 - \frac{a}{2R_0} x_2. \tag{4.17}$$

To model the static friction between the membrane and the surface of the channel we introduce μ that gives the friction force proportional to the normal force from the pressure. In section 4.2.1 we establish a condition without friction and in section 4.2.2 we add friction and discuss the results.

4.2.1 Without friction

Using eq.4.15 with eq.4.17 we have the expression of x_2 corresponding to the advancement inside the channel

$$x_2 = \frac{\beta\alpha}{2(1-\alpha)} 2R_0, \tag{4.18}$$

we introduce also $\beta = \frac{P}{k}$ (see fig.4.3). We establish $\alpha = \frac{a}{R_0}$ being the ratio between the constriction size and nucleus size R_0. The nucleus is fully inside when $x_1 = 0$. It gives us the condition on x_2 when the process is completed

$$x_{2max} = \frac{2R_0}{\alpha}, \tag{4.19}$$

combining eq.4.18 and eq.4.19 we obtain the equality

$$\frac{4}{\alpha} = \frac{\beta\alpha}{2(1-\alpha)}. \tag{4.20}$$

The eq.4.20 can be written in a polynomial form

$$\beta\alpha^2 + 2\alpha - 2 = 0, \tag{4.21}$$

the solution is given by

$$\alpha = \frac{\sqrt{1+2\beta} - 1}{\beta}. \tag{4.22}$$

The variable α gives the boundary between two phases (see fig.4.4). A phase where the nucleus is able to cross for a given (α, β) and not in the opposite phase under the curve. We remind that $0 < \alpha < 1$. We notice that for large values of β that the minimum value of α as shown in fig.4.4. In the case where $\alpha \to 1$ in eq.4.4 any value of $\beta > 0$ is sufficient to cross since we have no constriction. As the constriction gets smaller and smaller we need a greater pressure to be in the phase allowing the passage of the nucleus.

4.2.2 With static friction

We add to the model presented in section 4.2.1 a static friction force to depict a more general model especially at the interface. We show the presence of a critical value of μ_s for which no crossing is possible whatever the values of β is and $\alpha < 1$. Biologically this could lead in a real experiment to the rejection of the nucleus or the breaking of the membrane if the pressure exceeds the elastic and plastic regime. We start with the static friction force expression given by

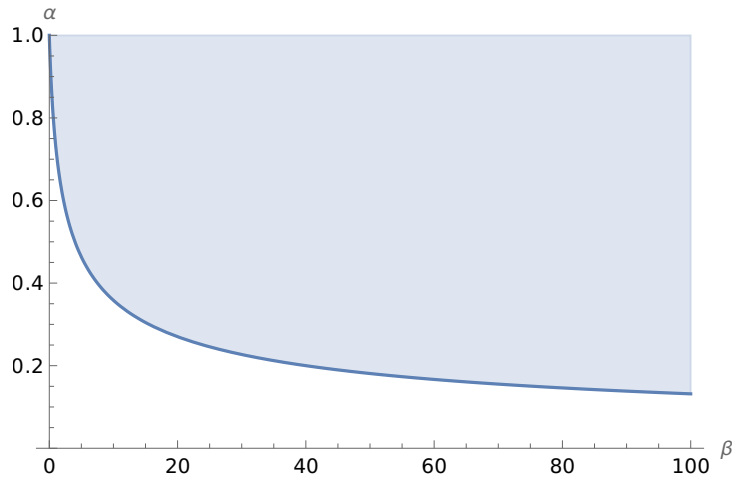

Figure 4.4: The blue area corresponds to the condition ($\alpha = \frac{a}{R_0}$,$\beta = \frac{P}{k}$) where the crossing is possible following our assumption. The larger the value of β the smaller can be the constriction.

$$F_{friction} = -2\mu_s P(x_1 + x_2 + R_0 - a), \tag{4.23}$$

we obtain the new sum of forces

$$Pa = k(x_1 + x_2 - 2R_0) + \mu_s P(x_1 + x_2 + R_0 - a). \tag{4.24}$$

We deduce x_2 with the same method as in section 4.2.1

$$x_2 = \beta \frac{\alpha R_0 - \mu_s(3R_0 - a)}{(1-\alpha)(1+\mu_s)} \tag{4.25}$$

and isolate $\alpha = \alpha(\mu_s, \beta)$ taking the condition $x_2 = \frac{2R_0}{\alpha}$

$$\frac{2R_0}{\alpha} = \beta \frac{\alpha R_0 - \mu(3R_0 - a)}{(1-\alpha)(1+\mu_s)}. \tag{4.26}$$

After simplification we end up with the polynomial

$$\beta(1+\mu_s)\alpha^2 + (2\mu_s + 2 - 3\mu_s\beta)\alpha - 2(1+\mu_s) = 0, \tag{4.27}$$

and solution

$$\alpha_\pm = \frac{-(2\mu_s + 2 - 3\mu_s\beta) \pm \sqrt{(2\mu_s - 3\mu_s\beta + 2)^2 + 8\beta(1+\mu_s)^2}}{2\beta(1+\mu_s)}. \tag{4.28}$$

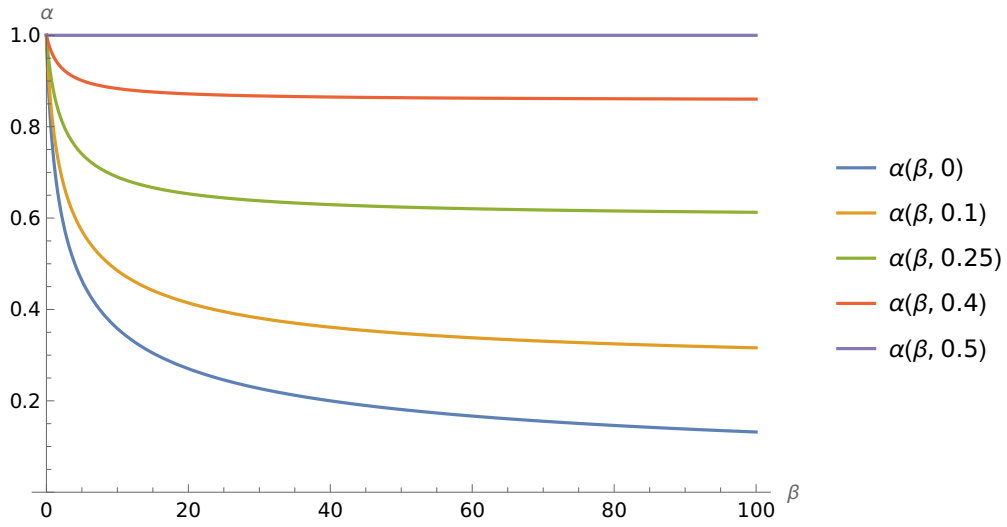

Figure 4.5: $\alpha(\beta)$ for different values of μ_s the coefficient of static friction. As we increase μ_s we need higher values of β for the the same value of α.

Keeping the physical value where $0 < \alpha < 1$ gives

$$\boxed{\alpha(\beta, \mu_s) = \frac{\sqrt{(2\mu_s - 3\mu_s\beta + 2)^2 + 8\beta(1+\mu_s)^2} - (2\mu_s + 2 - 3\mu_s\beta)}{2\beta(1+\mu_s)}}, \quad (4.29)$$

and for $\mu = 0$ we recover the result from section 4.2.1 in eq.4.22. The solution in eq.4.29 (see fig.4.5) has a limit for eq.4.29 when $\beta \to \infty$.

$$\alpha(\beta, \mu_s) \to \frac{3\mu_s}{(1+\mu_s)}. \quad (4.30)$$

4.3 Probability of crossing

4.3.1 Maximum elastic extension

Experimentally the crossing of a constriction with a given size entrance is not always totally deterministic in fact biological systems tend to be stochastic processes involving diffusion, temperature dependent chemical reactions and a variability in terms of size and shape. We observe that for a same size entrance $2a$ a different outcomes represented by a statistic. In this section we propose a model explaining predicting the probability of crossing with constriction size and statistics obtained experimentally [37]. We start first with a an elastic force model of the nucleus and in a second time the pressure generated by a density of single elements of force that we propose to be actin filament. It is from this

last element of the model that we introduce a random element that generates a probability. We start first with an observation of elastic force and pressure pushing. We can write the elastic force in a 1d form with K the elastic constant and x the position from equilibrium

$$F_{el} = -Kx, \tag{4.31}$$

x is the deformation of the nucleus in the tunnel. The force pushing to the inside of the tunnel coming from the pressure is

$$F_P = P\pi a^2 \tag{4.32}$$

and in order to be able to stay inside the tunnel the force pushing must be equal or greater than the elastic force

$$Pa^2 \geq Kx \tag{4.33}$$

keeping the nucleus from moving inside. We reach the maximum elongation when the equality is satisfied between elastic force and pressure force for

$$x_{eq} = \frac{Pa^2}{K}. \tag{4.34}$$

4.3.2 Elastic model

We assume that the elasticity K may depend on the characteristic size of the object for a shell type configuration. In the case of shell type nucleus with a very thin membrane with a thickness $h << a$ the constant K may scale following only the perimeter of the entrance with K_s the modulus of elasticity with $2\pi a$ the characteristic size of the elastic piece concerned by the deformation

$$K(a) = 2\pi a K_s. \tag{4.35}$$

Replacing in eq.4.34 the eq.4.35 gives the equilibrium length for the linear density case

$$x_{eql} = \frac{Pa}{2\pi K_s}. \tag{4.36}$$

It indicates that the larger the entrance a of the constriction leads to a higher estimate of x_{eql} in the channel.

4.3.3 Condition on the pressure P

In the following part we aim to establish the probability of crossing. To do so we search for condition to keep the nucleus in the tunnel after the constriction. Once we establish the condition we can introduce the scenario when the condition is not verified and leads to a failure in crossing. We have a first condition at the entrance found in section 4.1 with eq.4.7. On another hand the nucleus is filling the tunnel and we assume that the walls are pressing against the cell and

nucleus. In order to stay in the tunnel we suppose that the friction to balance the elastic force trying to bring back the nucleus out of the constriction. Taking an extension length of δ and K the elastic spring constant we have

$$F_{el} = -K\delta. \tag{4.37}$$

The friction from the pressure pushing from inside to the outside of the nucleus and the wall. This force is related to a static friction (see fig.4.6).

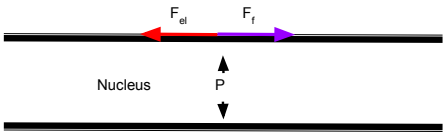

Figure 4.6: Nucleus in the channel against the walls with the two forces: F_{el} and F_f.

$$F_f = 2\pi a\delta\mu_s P. \tag{4.38}$$

Using eq.4.37 and eq.4.38 we can write the condition on static friction

$$2\pi\mu_s P a\delta > K\delta, \tag{4.39}$$

This leads to a condition on μ_s

$$\mu_s > \frac{K_s}{P}, \tag{4.40}$$

we now combine eq.4.7 with eq.4.40 to obtain a range for μ given by

$$\frac{K_s}{P} < \mu_s < \frac{\alpha^2}{1-\alpha^2}. \tag{4.41}$$

The lower boundary is purely intrinsic to the cell with its mechanical and force generation capacity. The softer and higher the capacity of the cell to generate pressure the easier it is to get into the constriction. For the upper boundary it is geometrical and the larger is the entrance the wider is the range for μ_s. The condition where the range is no longer possible corresponds to when the upper bound is equal to the lower bound or more as shown by

$$\frac{\alpha^2}{1-\alpha^2} < \frac{K_s}{P}, \tag{4.42}$$

the three variables (R_0, K_s, P) are completely determined by the cell approaching the constriction. For the following sections we take the minimum pressure

$P > P_{min}$ as a minimum to make the the nucleus able to stay in the tunnel after crossing the entrance given by eq.4.43

$$\boxed{P > K_s \frac{1-\alpha^2}{\alpha^2}}. \tag{4.43}$$

4.3.4 Distributed pressure

In the following section we assume that the pressure generated by the force from the cell is not fixed but rather distributed based on a heterogeneous density of filaments or any other single element generating force. In fact the model could be used for any force element. When needing values for force we may take the force and size and actin filaments.

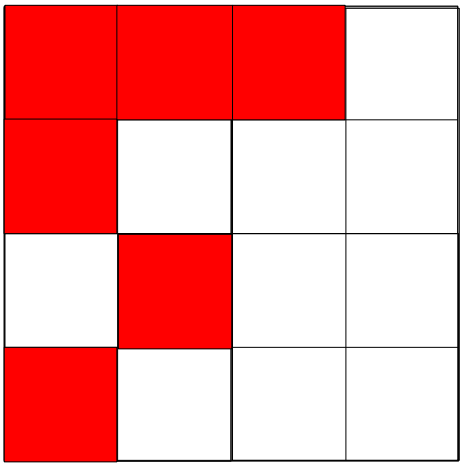

Figure 4.7: Element of surface decomposed into filament slots. Red squares indicate the presence of actin and white squares are empty. This illustrates the density fluctuation since the occupation of a site depends on probability p.

We assume that the density of actin during the process generates a pressure to push the nucleus in the constriction. The pressure follows a normal distribution with an average P_0 and a standard deviation σ_P

$$p(P) = \frac{1}{\sigma_P \sqrt{2\pi}} e^{-\frac{(P-P_0)^2}{2\sigma_P^2}}, \tag{4.44}$$

the condition to maintain the nucleus in the constriction for the nucleus requires

a minimum pressure P_{min}

$$P_{min} = K_s \frac{1-\alpha^2}{\alpha^2}. \tag{4.45}$$

In the case where $P >> 1$ and $\sigma_P < P_0$ we can approximate the integral on P following

$$\int_{-\infty}^{\infty} p(P)dP \approx \int_{0}^{\infty} p(P)dP. \tag{4.46}$$

Based on the distribution in eq.4.46 we can establish the probability to have a pressure P under P_{min} by integrating to obtain the probability associated

$$p(P < P_{min}) = 1 - \int_{P_{min}}^{\infty} p(P)dP, \tag{4.47}$$

we can substitute eq.4.44 and taking f as the force of an element of force that can occupy a site (see fig.4.7) in eq.4.47 we obtain

$$p(P < P_{min}) = 1 - \int_{P_{min}}^{\infty} \frac{1}{f\sigma_\rho\sqrt{2\pi}} e^{-\frac{(P-P_0)^2}{2f^2\sigma_\rho^2}} dP. \tag{4.48}$$

Integration gives $p_{failure}$, the probability to fail crossing

$$p_{failure} = 1 - \frac{1}{2}\left[erf\left(\frac{P-P_0}{\sqrt{2}f\sigma_\rho}\right)\right]_{P_{min}}^{\infty}, \tag{4.49}$$

$$p_{failure} = 1 - \frac{1}{2}\left(1 + erf\left(\frac{P_0 - P_{min}}{\sqrt{2}\sigma_P}\right)\right). \tag{4.50}$$

Using the expression in eq.4.51 and eq.4.50 we give the probability of crossing

$$p_{crossing} = 1 - p_{failure}, \tag{4.51}$$

$$p_{crossing} = \frac{1}{2}\left(1 + erf\left[\frac{P_0 - P_{min}}{\sqrt{2}\sigma_P}\right]\right). \tag{4.52}$$

We introduce for a better understanding the two following non-dimensional parameters:

- $\phi = \frac{P_{min}}{P_0}$. The parameter ϕ is the ratio between the pressure P_{min} necessary to maintain the crossing and P_0 the average pressure.
- $x = \frac{\sigma_P}{P_0}$. x corresponds to the ratio between the standard deviation and the average also called the coefficient of variation.

With the introduction of the two previous parameters we have can rewrite eq.4.52 (see fig.4.8)

$$p_{crossing}(x, \phi) = \frac{1}{2}\left(1 + erf\left[\frac{1-\phi}{x\sqrt{2}}\right]\right). \tag{4.53}$$

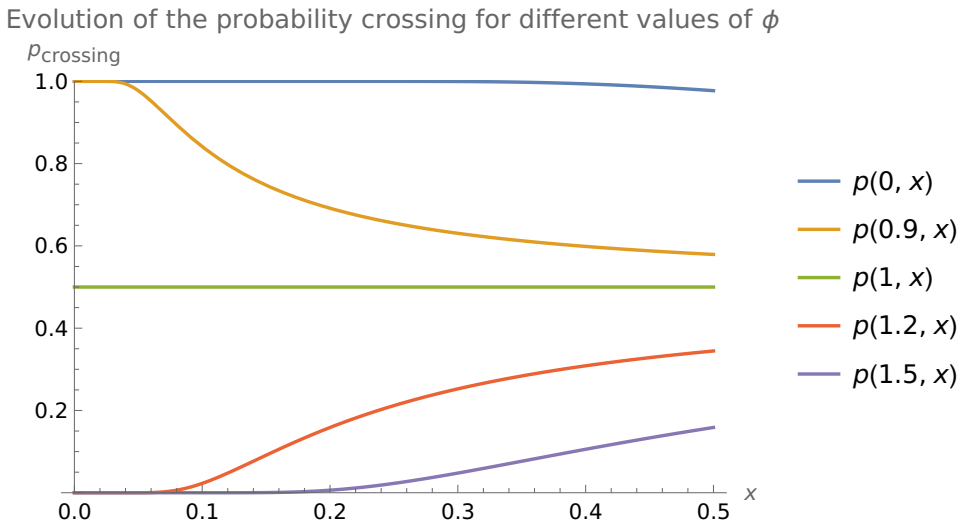

Figure 4.8: We consider in this figure a range for x between 0 and 0.5 for different values of $\phi = \frac{P_{min}}{P_0}$.

We plot also the evolution of this probability with ϕ for different values of x in fig.4.9. A higher the value of ϕ means that $P_{min}$is higher than the average pressure P_0 of the cell on the nucleus.

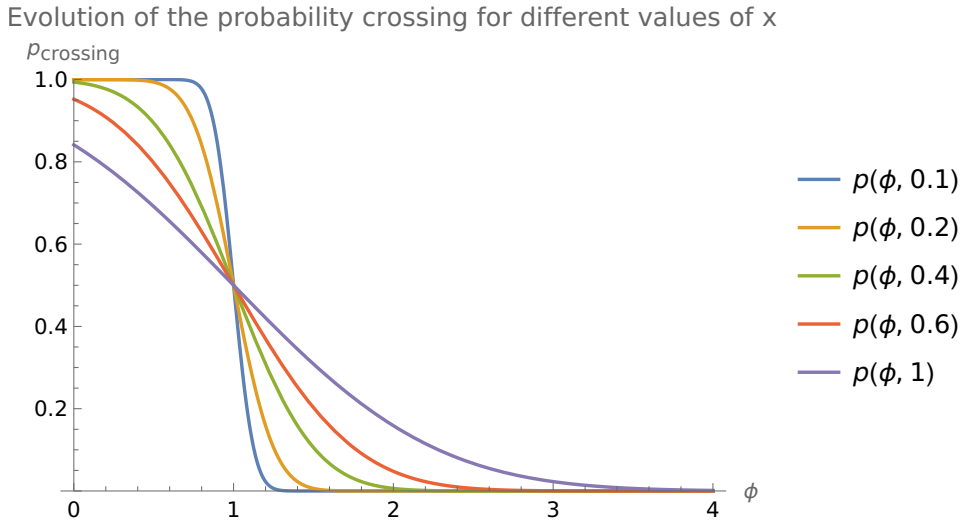

Figure 4.9: We consider here different values of x the coefficient of variation related to the fluctuation of the density.

Constriction size effect. From the two parameters x and ϕ we can relate

them to the constriction size a and taking $P_0 = f\rho_0$. We have for x

$$x = \frac{\sigma_\rho}{P_0} = \frac{f\sigma_\rho}{f\rho_0}, \tag{4.54}$$

taking $\sigma_\rho = \frac{1}{2\sqrt{\pi}al}$ and $\rho_0 = \frac{1}{2l^2}$ that we replace in eq.4.54 which gives

$$x = \frac{l}{a\sqrt{\pi}}. \tag{4.55}$$

The result means that the smaller is a and closer in magnitude to the size of a filament site the larger will be the coefficient of variation. We except a scenario when we reduce the size of the entrance a higher pressure P_{min} needed and a higher fluctuation of the force pushing to the inside of the tunnel.

We have ϕ that we can express as a function of a if we take $P_{min} = K_s\left(\frac{1-\alpha^2}{\alpha^2}\right)$. We introduce $g = \frac{P_0}{K_s}$ and have ϕ

$$\phi = \frac{1-\alpha^2}{g\alpha^2}, \tag{4.56}$$

taking this value of ϕ we can write $p(x, \alpha)$

$$p_{crossing}(x, \alpha) = \frac{1}{2}\left(1 + erf\left[\frac{1 - \frac{(1-\alpha^2)}{g\alpha^2}}{x\sqrt{2}}\right]\right). \tag{4.57}$$

We consider in the following the probability $p(\alpha)$ for different values of g and x to observe the effect of each one on $p(\alpha)$ using the expression(see fig.4.10 and fig.4.11)

$$p_{crossing}(a, x) = \frac{1}{2}\left(1 + erf\left[\frac{1 - \frac{1}{g}(\frac{1-\alpha^2}{\alpha^2})}{x\sqrt{2}}\right]\right). \tag{4.58}$$

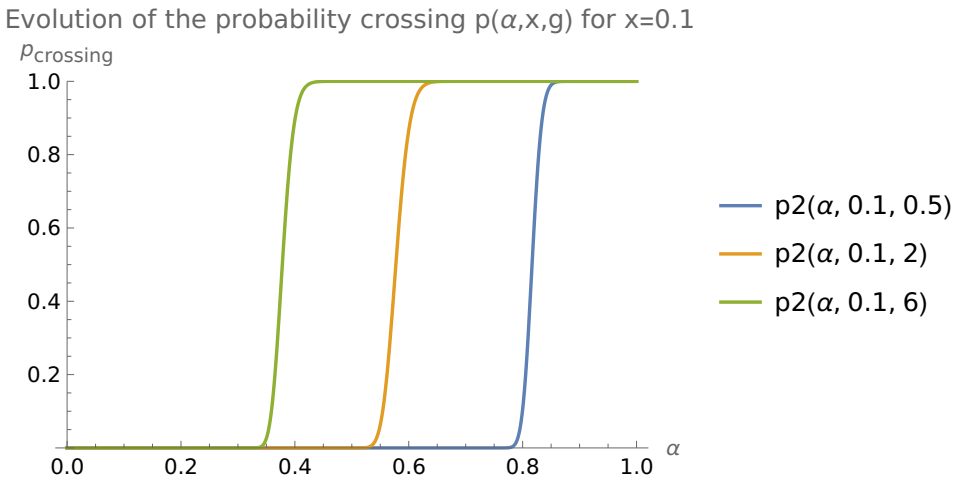

Figure 4.10: Changing g which corresponds to the ratio between average pressure and elasticity parameter K_s changes the value of the average pressure. We notice that when we have a larger pressure in green compared to the blue the minimum constriction size to have a realistic probability to cross can be smaller. The value of g changes the transition point between $p \to 0$ and $p \to 1$.

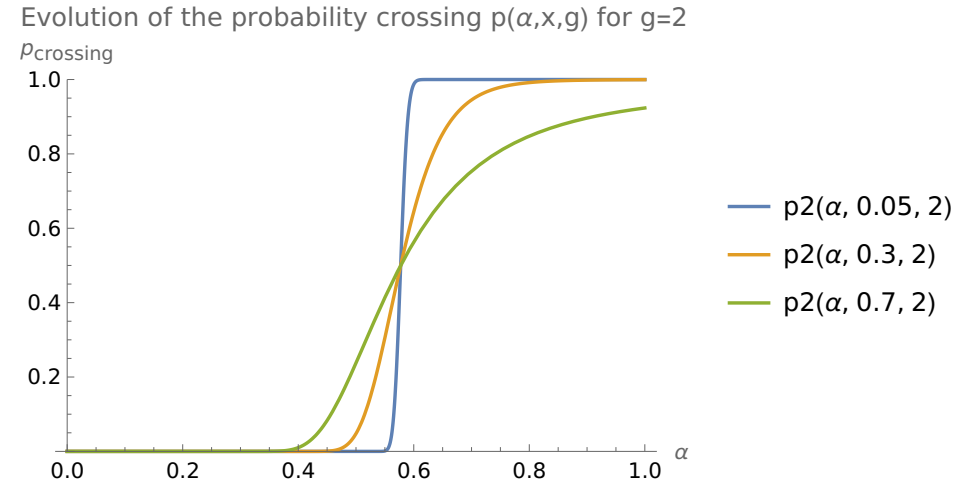

Figure 4.11: When $x << 1$ the probability increases sharply like a step function. By increasing the value of x we have a smoother transition.

σ_ρ as a function of a.

We add parameters to express our equations with physical parameters like a to the model by expressing σ_ρ with other parameters through the probability to occupy a site. In that case the size of the constriction is not explicitly present

since we consider that the first condition is always valid. Each force element from actin filaments or other possible sources like contraction is called f which is the force of a single element. The average density ρ_0 can be associated with a fluctuation following the average assuming a fluctuation in the force generated between each filament. Having the density ρ we have the total force given by eq.4.59.

$$F = \pi \rho_0 a^2 f \tag{4.59}$$

From the total force we deduce P in eq.4.60.

$$P = f\rho \tag{4.60}$$

The probability $p(P)$ is obtained by changing the variable

$$p(P) = p(\rho)\frac{d\rho}{dP}. \tag{4.61}$$

From the standard deviation σ_ρ we deduce the standard deviation σ_P on pressure

$$\sigma_P = f\sigma_\rho. \tag{4.62}$$

We take the value of σ_ρ as an expression of a and l. The variable l is the thickness of an actin filament for example or any element generating force. Each space of area l^2 can be empty or occupied as shown in fig.4.7. If we associate to a random variable i can take the value 0 or 1. The total number of filaments on the surface $S_a = \pi a^2$ is given by M in eq.4.63.

$$M = i_1 + ... + i_N \tag{4.63}$$

We sum over the N boxes that we can calculate knowing l given by eq.4.64.

$$N = \frac{S_a}{l^2} \tag{4.64}$$

For a circular entrance we take $S_a = \pi a^2$. The density ρ is given by eq.4.65 which is the number of elements M divided by the total area S_a.

$$\rho = \frac{M}{S_a} \tag{4.65}$$

We have for $Var(\rho)$:

$$Var(\rho) = \frac{1}{S_a^2}Var(M) = \frac{Var(i_1 + ... + i_N)}{S_a^2} = \frac{NVar(i)}{S_a^2} \tag{4.66}$$

By replacing the total number of emplacements $N = \frac{S_a}{l^2}$ and $Var(i) = p_1(1-p_1)$ with p_1 the probability to occupy an emplacement.

$$Var(\rho) = \frac{p_1(1-p_1)}{S_a l^2} \tag{4.67}$$

Taking the expression $S_a = \pi a^2$ and $Var\rho = \sigma_\rho^2$ we obtain the standard deviation for the density ρ to use it in section 4.3.5 for x

$$\sigma_\rho = \frac{\sqrt{p_1(1-p_1)}}{\sqrt{\pi} a l} \tag{4.68}$$

4.3.5 Probability and variance with temperature and energy.

We aim to express the parameters in the probability of crossing with physical parameters like constriction size, force for example and energy. We consider that to occupy a space on the surface we need an energy U, once the site is occupied we consider the force, and that two states are possible:

- State 1: Occupied emplacement with an energy U and a probability p_1.
- State 0: Empty state that doesn't require energy since it is the initial state of all sites with a probability p_0.

Taking a Boltzmann probability distribution to describe the probability related to both states and the respective energy associated $E = U$ and $E = 0$ (See fig.4.12)

$$p_0 = \frac{e^{0\beta}}{1 + e^{-\beta U}} = \frac{1}{1 + e^{-\beta U}}, \tag{4.69}$$

$$p_1 = \frac{e^{-\beta U}}{1 + e^{-\beta U}}. \tag{4.70}$$

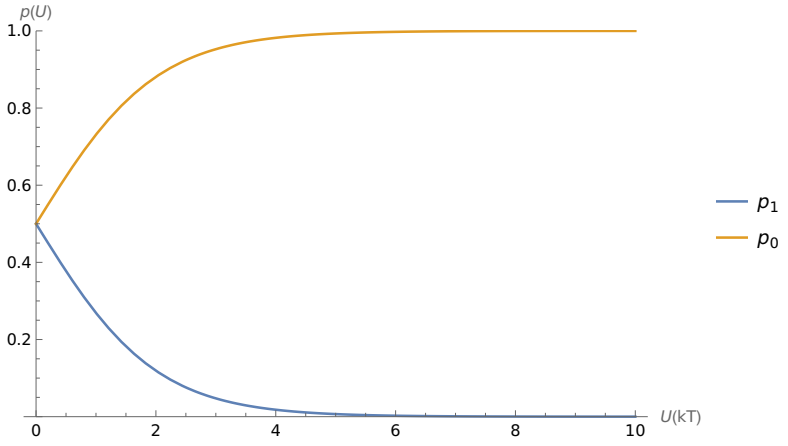

Figure 4.12: Evolution of the probability with U in unit of kT. The higher is the energy cost U to add an element of force the lower is the probability p_1 to find an occupied site.

We replace the expression of p_1 of eq.4.70 in eq.4.68 we can deduce the standard deviation $\sigma_P = f\sigma_\rho$

$$\sigma_P = \frac{f}{\sqrt{\pi}al}\sqrt{\frac{e^{-\beta U}}{1+e^{-\beta U}}\left(1-\frac{e^{-\beta U}}{1+e^{-\beta U}}\right)} = \frac{f}{al\sqrt{\pi}}\frac{e^{-\beta U/2}}{1+e^{-\beta U}}, \tag{4.71}$$

and given the average pressure

$$P_0 = \frac{Np_1 f}{\pi a^2} = \frac{\pi a^2 p_1 f}{l^2 \pi a^2} = \frac{p_1 f}{l^2} \tag{4.72}$$

we can finally give $x = \frac{\sigma_P}{P_0}$ using eq.4.71 and eq.4.72

$$x = \frac{l}{a\sqrt{\pi}p_1}\frac{e^{-\beta U/2}}{1+e^{-\beta U}}. \tag{4.73}$$

Replacing p_1 by eq.4.70 gives the final expression for x

$$\boxed{x = \frac{l}{a\sqrt{\pi}}e^{\beta U/2} = \frac{l}{R_0\alpha\sqrt{\pi}}e^{\beta U/2}}. \tag{4.74}$$

We define $\lambda = \frac{l}{R_0}$. We replace now x in eq.4.58 to obtain eq.4.75

$$p_{crossing}(\alpha) = \frac{1}{2}\left(1 + erf\left[\sqrt{\frac{\pi}{2}}\frac{\alpha e^{-u/2}(1-\frac{(1-\alpha^2)}{g\alpha^2})}{\lambda}\right]\right) \tag{4.75}$$

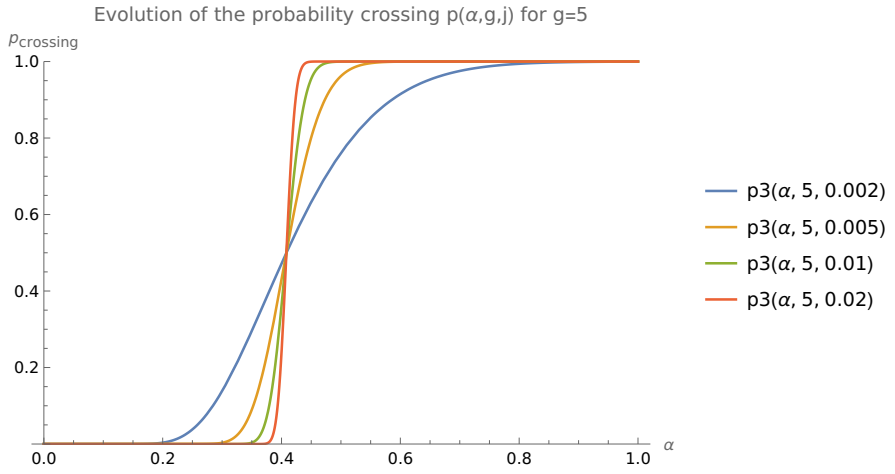

Figure 4.13: Evolution of the probability for different values of $j = e^{-u/2}$ and $g = 5$ with $u = U\beta$.

Expressing P_0 the average pressure with p_1.

We can rewrite the parameter g using

$$g = \frac{P_0}{K_s} = \frac{f}{K_s l^2} p_1, \tag{4.76}$$

we introduce δ and replace p_1 in eq.4.76

$$\delta = \frac{f}{K_s l^2}, \tag{4.77}$$

$$g = \delta \frac{e^{-u}}{1 + e^{-u}}. \tag{4.78}$$

The obtained equation

$$p_{crossing}(\alpha, \delta, j) = \frac{1}{2}\left(1 + erf\left[\sqrt{\frac{\pi}{2}}\frac{\alpha}{\lambda} e^{-u/2}\left(1 - \frac{(1+e^u)(1-\alpha^2)}{\delta\alpha^2}\right)\right]\right) \tag{4.79}$$

can be rewritten using $j = e^{-u/2}$ to finally the expression of the probability with (see fig.4.14 and fig.4.15)

$$p_{crossing}(\alpha, \delta, j) = \frac{1}{2}\left(1 + erf\left[\sqrt{\frac{\pi}{2}}\frac{\alpha}{\lambda} j\left(1 - \frac{(1+\frac{1}{j^2})(1-\alpha^2)}{\delta\alpha^2}\right)\right]\right). \tag{4.80}$$

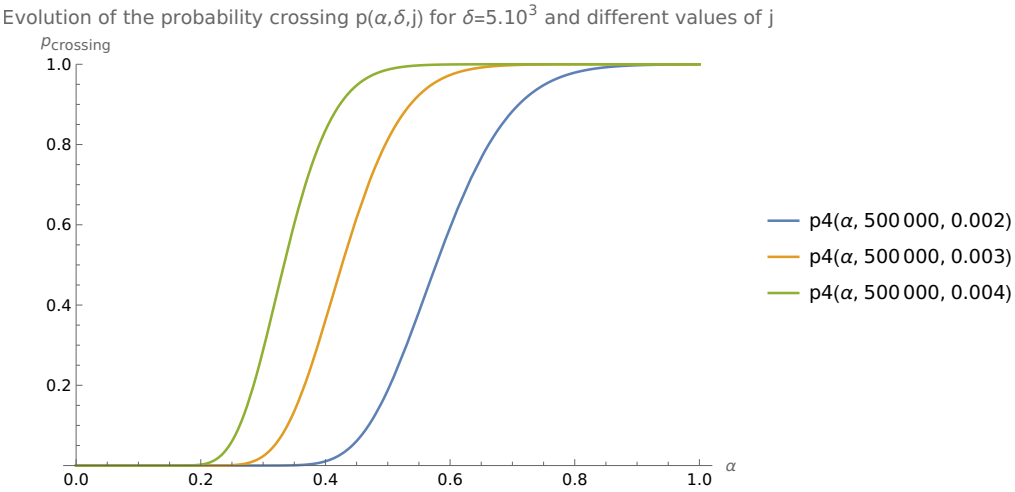

Figure 4.14: Evolution of the probability for different values of $j = e^{-u/2}$ and $g = 5$ with $u = U\beta$. $\lambda = 10^{-3}$.

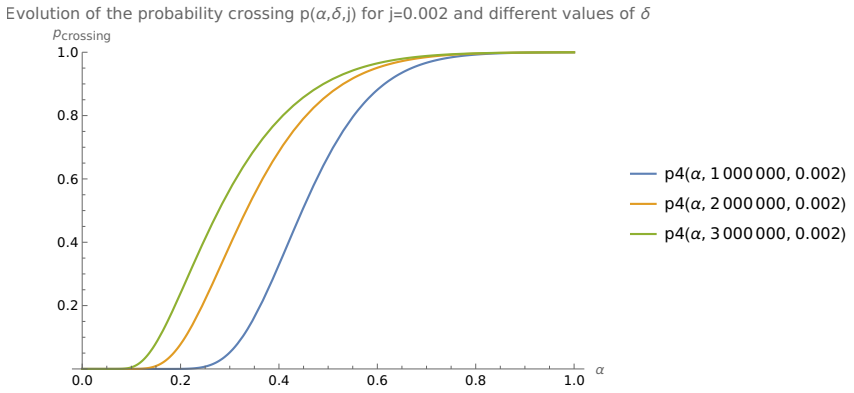

Figure 4.15: Evolution of the probability for different values of $j = e^{-u/2}$ and $g = 5$ with $u = U\beta$. $\lambda = 10^{-3}$.

4.3.6 Data fitting

Taking the value for the percentage of crossing given by [37] we perform a fit with the expression of the probability of crossing given by eq.4.80. We let j and δ as free parameters to estimate with the curve fit. The result is given by fig.4.16.

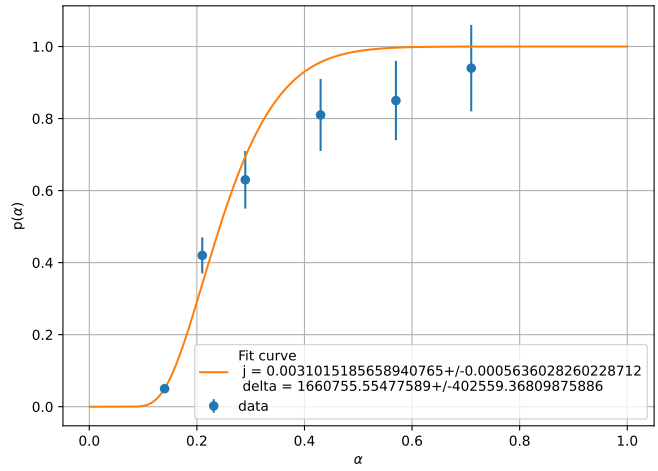

Figure 4.16: Curve fitting the data taken from [37] and representing the statistic of crossing nucleus with the probability $p(\alpha)$ as we change the size of the constriction α.

Given the estimation of $j \approx 0.003$ and the expression

$$u = -2 \ln j, \tag{4.81}$$

we can deduce the value for u in

$$u \approx 11.6. \tag{4.82}$$

In units of kT

$$U \approx 11.6kT. \tag{4.83}$$

The standard deviation is derived from

$$du = -\frac{2}{j} dj \tag{4.84}$$

and gives an expression for u with the associated error

$$\boxed{u = 11.6 \pm 0.4}. \tag{4.85}$$

The value of δ given by eq.4.77 is used to estimate K considering the estimate of $\delta \approx 10^6$

$$\boxed{K \approx \frac{2\pi 10^{-6} 10^{-11}}{10^6 10^{-18}} \approx 6 \times 10^{-5} N/m}. \tag{4.86}$$

The value when compared to the value measured in [35] and is discussed in the summary. We took $a = 10^{-6}m$, the force $f = 10^{-11}N$ and $l = 10^{-9}m$.

4.4 Summary

We have started this chapter with a 2d model to predict the possible configurations allowing a crossing into a constriction. The parameters that we highlighted as crucial for crossing are geometrical like nucleus and constriction sizes and on another hand we have the pressure and elasticity that are mechanical. It appeared also that there is an ideal value for μ allowing crossing. Then we introduced a model requiring a minimum pressure to maintain the crossing and defined the condition of a failure for the nucleus to keep migrating in the tunnel. Having a minimum pressure required and pressure distribution pushing the nucleus introduces a probability of failure or success. We finally related to the distribution the key parameters of our problem and associated each force element generating the pressure to an energy cost with its probability of presence to depict an inhomogeneous density giving rise to a distributed pressure that changes with the constriction size. To that result we have been able to compare our theory with observations given in [37]. The elasticity estimated was also compared with [35] and was lower but it is important to point that the elasticity is non-linear which is a property that we didn't take into account in our model. Moreover [10] showed a that the shell structure of the nucleus is closer to reality than a full body. The addition of normal forces to the movement that can help introduce the cell in the constriction were not added and could allow a stiffer nucleus.

Chapter 5

Conclusion

We started the present work by presenting first the cell and its main components with a central role in its mechanical properties. We identified the nucleus, lipid bilayer and cortex as the main elastic materials during deformations. Cell reshaping is necessary for endocytosis process and cell migration in constrictions and we were motivated by the impact of elastic properties and the force generated by the cell. Observations from experiments appeared to indicate a particular size preferred for internalisation when counting the total number of beads internalised. The interpretation given to this result was that the energy may show a minimum with target size facilitating the uptake by the cell. Even if this assumption may be tempting and straightforward it may not be as easy as it seems. We took first the case of phagocytosis and the energy required to reshape the lipid bilayer membrane using Helfrich formulation for bending energy in the case of a sphere but it did not appear to us that the energy had a minimum for bead radius $R \neq 0$. On the contrary of spherocylinder wrapping showing a minimum dependent on the length for the bending energy deformation. We have next presented an approach taking the cortex under the lipid bilayer with an excluded volume interaction in a case of high curvature. In fact the thickness of the cortex (few hundred nanometres) is very close to the bead size of interest (see table 1.1). The result obtained (see section 2.4.2) revealed a central role of cortex thickness and the range of the interaction obtained. This points out the role of the cortex during reshaping and the necessity to better understand endocytosis processes. Another observation on cortex thickness is that if we assume more force required to bend a target with a high curvature this would mean a thicker cortex and as we have seen in section 2.4.2 moves the minimum. We can expect a limit between a cortex thick enough to generate force and not too thick which would increase the position of the minimum of energy and smaller targets would be missed. Experiments around cortex structure and interaction with the lipid bilayer, like spacing [9] (reviewed in [8]), will help to make better predictions on that aspect.Finally we built a model based on two probabilities: the probability of finding bead and the probability to cross the energy barrier to form the phagocytic cup leading to full engulfment (see

section 2.5). We showed the existence of a size maximising the probability of uptake. The model revealed also the necessity of adding a source of energy helping the reshaping and engulfment that increases with the size of the bead to allow a more consistent estimate of the bending modulus with the literature. Regarding target shape, prolate shape exhibits a preferred curvature when they encounter a macrophage making it easier to take up but too highly curved or a too flat shapes and it reduces the take up capacity of the cell.The two models are not excluding and could be considered at the same time.

In chapter 3 we proposed a dynamical model that introduces a feedback loop to the final stage of engulfment that has been observed as much faster compared to the first step of engulfment in the case of a spherical target. We aimed to show that an approach not requiring diffusion and drift for receptors binding the target and the membrane (see [12] [29] [28]) to show a different possibility that can be investigated further. The process includes the viscous property of the cortex combined to the pressure generated by the actomyosin on the target to take up. The two properties of the cortex: force generation and viscosity are the limiting factors to the phagocytosis rate concerning the second phase of engulfment. Moreover this mechanism can be used for the description of an incompressible fluid i.e. the case of macropinocytosis (see section 1.3.3) since it doesn't require a hard body with any coating on it to take place. The contribution from thermal fluctuation, the element of energy k_bT from the environment to the cell to any form of energy (chemical or Brownian motion), plays a role following our model to break the symmetry of the initial condition and give the initial "kick" to start the process. Two main assumptions have been made to get an analytical solution. The first is that the bead is large compared to the phagocytic pseudopod forming the cup surrounding the bead. The second assumption was to take the flow as not explicitly time dependent which means that we go from a stationary state to another stationary state as the pressure changes with the progression of the engulfment.

In chapter 4 we focused on the nucleus which is the stiffer element of the cell in a situation of constriction crossing. A situation that can be encountered during cell migration, for example when moving through constrictions like pores or small capillaries, with a complete crossing requiring a reshaping of the nucleus. Getting over the elastic energy barrier and the friction around the nucleus are the main obstacles to the movement in order to enter the constriction. In our model we assumed a friction and an elasticity from the nucleus in the migration as the main limiting object in the cell being stiffer. A first condition to move forward based on static friction (eq.4.6) and on another hand we have assumed the friction to be necessary to keep the elastic nucleus in the tunnel and avoid a pull back which we consider as a failure to cross (eq.4.40). We established a range on the value of μ, the static friction, leading to a condition on the pressure applied on the nucleus to move in the constriction. We used a pressure that follows a Gaussian distribution (see eq.4.44) with an average and variance calculated from the force elements (see fig.4.7). Since the total force on the surface pushing is not predictable we end up with a probability for the pressure hence the distribution of the possible values of P. We pictured the surface density

of force elements into small elements of surface that can be occupied with an energy cost and thermal fluctuations. The straightforward possibility is to see it as an actin filament but in theory other scenarios could be considered. We ended up with a crossing probability that can be compared to results from [37] to estimate the parameters left unknown: the energy cost in the density model with the elasticity of the nucleus. The result obtained for the energy seemed reasonable for a process at that scale i.e. few kT. Regarding the nucleus elasticity our result indicated a softer object but can be explained by the lack of extra forces especially on the lateral sides [10] of the nucleus. Another effect that our model is not able to catch is from non linear elastic response or heterogeneous nucleus with a rigid lamina and a softer chromatin for example. Possible further work will be explored in the outlook. We also give an updated version of fig.1.5 in fig.5.

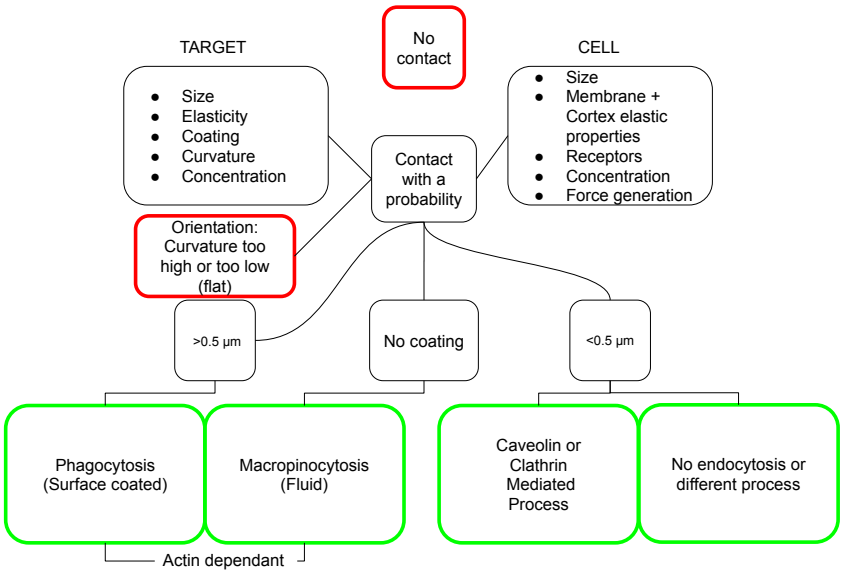

Figure 5.1: Updated diagram(see fig.1.5). The red boxes describe the failure of the cell to perform a complete engulfment. The green boxes indicates the successful outcomes leading to internalisation.

Chapter 6

Outlook

We give in this chapter some further ideas to explore for each chapter.

6.1 Considering more cases with phagocytosis

We can take into account the extra pieces of membrane that can be added through exocytosis. A possibility is to associate with each vesicle generated for exocytosis an energy cost or by considering a limited reservoir of vesicles for example. The difficulty will come from the formulation of the energy. A possibility would be to evaluate the energy for each vesicle with a fixed size. Concerning the shape of the target to take up more complex shapes which means less symmetric than a sphere or a spherocylinder. For example oblate or prolate objects which may require combining numerical work and orientation to see the influence of the local curvature when it is in contact with the macrophage making it even harder to predict since the curvature changes on the surface. The calculation method for the spherocylinder in section 2.7 can be used as a starting point for other shapes.

Concerning the excluded volume (see section2.4) we took a very simple model to describe the energy associated. It would be more realistic to consider the interaction for the whole volume of the cortex. A better knowledge on the cortex structure can help and requires better imaging. For section 2.5 we considered in our case that after a successful phagocytosis we don't distinguish between the cells and assume that R_0 is the same even after a large number of beads. Furthermore having a decreasing number of beads would change the concentration and the probability to find a bead. Lastly we notice that since phagocytosis and macropinocytosis are both actin mediated, it would be interesting to state on the distribution of vesicle sizes formed by phagocytosis. In fact since that there is no coating needed it would be possible to know if there is also a preferred size vesicle when the engulfment is not bound by a coated surface to follow. It may give a better understanding on the role of the cortex with target size.

6.2 Taking the model further with a numerical work

We can propose a numerical model to solve the fluid dynamics around a sphere or even a less symmetrical object like a spherocylinder that takes into account the coupling with the pressure in a time dependant equation. This would allow us to have a better idea of the influence from eccentricity on the time needed to close the phagosome. The pressure may change, as we close the cup, differently compared to the sphere because the geometry is different. The pressure could increase quicker at the starting point for an oblate than a prolate. Our flow model doesn't exclude another process in parallel like a diffusion process for receptor ligand model(see [12][29][28]) and consequently the combination of both models could be tried.Another aspect of the engulfment that we neglected would be the elasticity of the membrane and would be more realistic especially for larger beads with a radius close to the cell size.

6.3 Adding non linear elasticity to the model

Taking a non-linear elastic force to describe the nucleus in chapter 4 would be interesting for example and see how it affects the possibility of crossing. For example taking an increasing elastic constant as we deform the nucleus and even adding a rupture point where the elastic force drops. Depending on the modelling of the nucleus we may expect a different shape deformation. Considering the chromatin in the nucleus as viscoelastic object with a relaxation time instead of a pure elastic object can be a way to get a more sophisticated model by catching the viscous effect with a relaxation time. The elastic properties of chromatin could be based on a model representing the DNA as multiple polymers with elastic properties. Moreover modelling the nucleus with two distinct value (as suggested in [35]) of elasticity as we pull the nucleus could reveal other unexpected behaviours during crossing.

Bibliography

[1] Bruce Alberts. *Molecular biology of the cell*. 2015. ISBN: 9781315735368.

[2] Amir H. Bahrami et al. "Wrapping of nanoparticles by membranes". In: *Advances in Colloid and Interface Science* 208 (June 2014), pp. 214–224. ISSN: 0001-8686. DOI: 10.1016/J.CIS.2014.02.012.

[3] D. Bochicchio and L. Monticelli. "The Membrane Bending Modulus in Experiments and Simulations: A Puzzling Picture". In: *Advances in Biomembranes and Lipid Self-Assembly* 23 (Jan. 2016), pp. 117–143. ISSN: 2451-9634. DOI: 10.1016/BS.ABL.2016.01.003.

[4] James Bradford. "Modelling actin polymerisation and phagocytosis". Feb. 2021. URL: https://etheses.whiterose.ac.uk/28555/.

[5] Jaime Obguia Cañedo. "The ultrastructural features of the surface of macrophages and the mechanics of phagocytosis". Feb. 2022. URL: https://etheses.whiterose.ac.uk/30348/.

[6] Julie A. Champion and Samir Mitragotri. "Role of target geometry in phagocytosis". In: *Proceedings of the National Academy of Sciences of the United States of America* 103 (13 Mar. 2006), pp. 4930–4934. ISSN: 00278424. DOI: 10.1073/PNAS.0600997103/SUPPL_FILE/00997FIG6.JPG. URL: https://www.pnas.org/doi/abs/10.1073/pnas.0600997103.

[7] Julie A. Champion, Amanda Walker, and Samir Mitragotri. "Role of particle size in phagocytosis of polymeric microspheres". In: *Pharmaceutical Research* 25 (8 Aug. 2008), pp. 1815–1821. ISSN: 07248741. DOI: 10.1007/S11095-008-9562-Y/FIGURES/5. URL: https://link.springer.com/article/10.1007/s11095-008-9562-y.

[8] Priyamvada Chugh and Ewa K. Paluch. "The actin cortex at a glance". In: *Journal of Cell Science* 131 (14 July 2018). ISSN: 14779137. DOI: 10.1242/JCS.186254/56817. URL: https://journals.biologists.com/jcs/article/131/14/jcs186254/56817/The-actin-cortex-at-a-glance.

[9] M. P. Clausen et al. “Dissecting the actin cortex density and membrane-cortex distance in living cells by super-resolution microscopy”. In: *Journal of Physics D: Applied Physics* 50 (6 Jan. 2017), p. 064002. ISSN: 0022-3727. DOI: 10.1088/1361-6463/AA52A1. URL: https://iopscience.iop.org/article/10.1088/1361-6463/aa52a1%20https://iopscience.iop.org/article/10.1088/1361-6463/aa52a1/meta.

[10] Ian D. Estabrook et al. “Calculation of the force field required for nucleus deformation during cell migration through constrictions”. In: *PLOS Computational Biology* 17 (5 May 2021), e1008592. ISSN: 1553-7358. DOI: 10.1371/JOURNAL.PCBI.1008592. URL: https://journals.plos.org/ploscompbiol/article?id=10.1371/journal.pcbi.1008592.

[11] D.A.D. Flormann et al. “The structure and mechanics of the cell cortex depend on the location and adhesion state”. In: *Proceedings of the National Academy of Sciences* 121.31 (July 2024). © 2024 the Author(s). Published by PNAS. This article is distributed under Creative Commons Attribution-NonCommercial-NoDerivatives License 4.0 (CC BY-NC-ND). (https://creativecommons.org/licenses/by-nc-nd/4.0/). URL: https://eprints.whiterose.ac.uk/218437/.

[12] Huajian Gao, Wendong Shi, and Lambert B. Freund. “Mechanics of receptor-mediated endocytosis”. In: *Proceedings of the National Academy of Sciences of the United States of America* 102 (27 July 2005), pp. 9469–9474. ISSN: 00278424. DOI: 10.1073/PNAS.0503879102/ASSET/AE8CEB39-BE90-4499-8561-326793969E7B/ASSETS/GRAPHIC/ZPQ0260586500005.JPEG. URL: https://www.pnas.org/doi/abs/10.1073/pnas.0503879102.

[13] Anusha Garapaty and Julie A. Champion. “Tunable particles alter macrophage uptake based on combinatorial effects of physical properties”. In: *Bioengineering & Translational Medicine* 2 (1 Mar. 2017), p. 92. ISSN: 2380-6761. DOI: 10.1002/BTM2.10047. URL: /pmc/articles/PMC5689517/%20/pmc/articles/PMC5689517/?report=abstract%20https://www.ncbi.nlm.nih.gov/pmc/articles/PMC5689517/.

[14] Stephanie E.A. Gratton et al. “The effect of particle design on cellular internalization pathways”. In: *Proceedings of the National Academy of Sciences of the United States of America* 105 (33 Aug. 2008), pp. 11613–11618. ISSN: 00278424. DOI: 10.1073/PNAS.0801763105/SUPPL_FILE/0801763105SI.PDF. URL: https://www.pnas.org/doi/abs/10.1073/pnas.0801763105.

[15] Hicheme Hadji and Kawthar Bouchemal. “Effect of micro- and nanoparticle shape on biological processes”. In: *Journal of Controlled Release* 342 (Feb. 2022), pp. 93–110. ISSN: 0168-3659. DOI: 10.1016/J.JCONREL.2021.12.032.

[16] Maurice B. Hallett. “An Introduction to Phagocytosis”. In: *Molecular and Cellular Biology of Phagocytosis*. Ed. by Maurice B. Hallett. Cham: Springer International Publishing, 2020, pp. 1–7. ISBN: 978-3-030-40406-2.

DOI: 10.1007/978-3-030-40406-2_1. URL: https://doi.org/10.1007/978-3-030-40406-2_1.

[17] W. Helfrich. "Elastic properties of lipid bilayers: theory and possible experiments". In: *Zeitschrift fur Naturforschung. Teil C: Biochemie, Biophysik, Biologie, Virologie* 28 (11 Dec. 1973), pp. 693–703. ISSN: 0341-0471. DOI: 10.1515/ZNC-1973-11-1209. URL: https://pubmed.ncbi.nlm.nih.gov/4273690/.

[18] Paul Janmey and Christoph Schimdt. "Cytoskeletal mechanics : models and measurements in cell mechanics". In: 2006. Chap. Experimental measurements of intracellular mechanics. ISBN: 9780511248795.

[19] Roger D. Kamm and Mohammad R.K. Mofrad. "Cytoskeletal mechanics : models and measurements in cell mechanics". In: 2006. Chap. Introduction, with the biological basis for cell mechanics. ISBN: 9780511248795.

[20] L. D. Landau and E. M. Lifshitz. *Course of Theoretical Physics, vol. 7, Theory of Elasticity, Landau and Lifshitz*. Vol. 7. 1986, p. 195. ISBN: 075062633X.

[21] Ines Lüchtefeld et al. "Elasticity spectra as a tool to investigate actin cortex mechanics". In: *Journal of Nanobiotechnology* 18 (1 Dec. 2020), pp. 1–11. ISSN: 14773155. DOI: 10.1186/S12951-020-00706-2/FIGURES/5. URL: https://jnanobiotechnology.biomedcentral.com/articles/10.1186/s12951-020-00706-2.

[22] James L. McGrath and C. Forbes Dewey. "Cell dynamics and the actin cytoskeleton". In: *Cytoskeletal Mechanics: Models and Measurements in Cell Mechanics*. Ed. by Mohammad R. K. Mofrad and Roger D.Editors Kamm. Cambridge Texts in Biomedical Engineering. Cambridge University Press, 2006, pp. 170–203.

[23] Lorraine Montel, Léa Pinon, and Jacques Fattaccioli. "A Multiparametric and High-Throughput Assay to Quantify the Influence of Target Size on Phagocytosis". In: *Biophysical Journal* 117 (3 Aug. 2019), pp. 408–419. ISSN: 0006-3495. DOI: 10.1016/J.BPJ.2019.06.021.

[24] Barrett O'Neill. *Elementary differential geometry*. eng. Rev. 2nd ed. Burlington, MA ; San Diego, CA ; London: Academic Press, an imprint of Elsevier, 2006. Chap. 5. ISBN: 9780080505428.

[25] Ben Ovryn, Terrance T. Bishop, and Diego Krapf. "Physics of the Cell Membrane". In: 2022, pp. 147–172. DOI: 10.1007/978-3-030-98606-3_6.

[26] Debjani Paul et al. "Phagocytosis Dynamics Depends on Target Shape". In: *Biophysical Journal* 105 (5 Sept. 2013), pp. 1143–1150. ISSN: 0006-3495. DOI: 10.1016/J.BPJ.2013.07.036.

[27] Laura Picas, Felix Rico, and Simon Scheuring. "Direct measurement of the mechanical properties of lipid phases in supported bilayers". In: *Biophysical journal* 102.1 (2012), pp. L01–L03.

[28] David M. Richards and Robert G. Endres. "How cells engulf: a review of theoretical approaches to phagocytosis". In: *Reports on Progress in Physics* 80 (12 Oct. 2017), p. 126601. ISSN: 0034-4885. DOI: 10.1088/1361-6633/AA8730. URL: https://iopscience.iop.org/article/10.1088/1361-6633/aa8730%20https://iopscience.iop.org/article/10.1088/1361-6633/aa8730/meta.

[29] David M. Richards and Robert G. Endres. "The Mechanism of Phagocytosis: Two Stages of Engulfment". In: *Biophysical Journal* 107 (7 Oct. 2014), p. 1542. ISSN: 15420086. DOI: 10.1016/J.BPJ.2014.07.070. URL: /pmc/articles/PMC4190621/%20/pmc/articles/PMC4190621/?report=abstract%20https://www.ncbi.nlm.nih.gov/pmc/articles/PMC4190621/.

[30] Rhiannon E. Roberts, Sharon Dewitt, and Maurice B. Hallett. "Membrane Tension and the Role of Ezrin During Phagocytosis". In: *Molecular and Cellular Biology of Phagocytosis*. Ed. by Maurice B. Hallett. Cham: Springer International Publishing, 2020, pp. 83–102. ISBN: 978-3-030-40406-2. DOI: 10.1007/978-3-030-40406-2_6. URL: https://doi.org/10.1007/978-3-030-40406-2_6.

[31] Samuel A. Safran. "Statistical thermodynamics of surfaces, interfaces, and membranes". In: 2003. Chap. Chapter 6. Flexible Interfaces. Fluid membranes. ISBN: 9780429976766.

[32] Gilbert Salloum, Anne R. Bresnick, and Jonathan M. Backer. "Macropinocytosis: mechanisms and regulation". In: *Biochemical Journal* 480.5 (Mar. 2023), pp. 335–362. ISSN: 0264-6021. DOI: 10.1042/BCJ20210584. eprint: https://portlandpress.com/biochemj/article-pdf/480/5/335/944325/bcj-2021-0584c.pdf. URL: https://doi.org/10.1042/BCJ20210584.

[33] R. Simson et al. "Membrane Bending Modulus and Adhesion Energy of Wild-Type and Mutant Cells of Dictyostelium Lacking Talin or Cortexillins". In: *Biophysical Journal* 74 (1 Jan. 1998), pp. 514–522. ISSN: 0006-3495. DOI: 10.1016/S0006-3495(98)77808-7.

[34] J. Spurk and N. Aksel. *Fluid Mechanics*. Springer Berlin Heidelberg, 2008. Chap. 13. ISBN: 9783540735366. URL: https://books.google.co.uk/books?id=7_FrhazRTgsC.

[35] Andrew D. Stephens et al. "Chromatin and lamin A determine two different mechanical response regimes of the cell nucleus". In: *Molecular Biology of the Cell* 28 (14 July 2017), p. 1984. ISSN: 19394586. DOI: 10.1091/MBC.E16-09-0653. URL: /pmc/articles/PMC5541848/%20/pmc/articles/PMC5541848/?report=abstract%20https://www.ncbi.nlm.nih.gov/pmc/articles/PMC5541848/.

[36] Yasuhiko Tabata and Yoshito Ikada. "Effect of the size and surface charge of polymer microspheres on their phagocytosis by macrophage". In: *Biomaterials* 9 (4 July 1988), pp. 356–362. ISSN: 0142-9612. DOI: 10.1016/0142-9612(88)90033-6.

[37] Hawa Racine Thiam et al. "Perinuclear Arp2/3-driven actin polymerization enables nuclear deformation to facilitate cell migration through complex environments". In: *Nature Communications 2016 7:1* 7 (1 Mar. 2016), pp. 1–14. ISSN: 2041-1723. DOI: 10.1038/ncomms10997. URL: https://www.nature.com/articles/ncomms10997.

[38] Daan Vorselen, Ramon Lorenzo D. Labitigan, and Julie A. Theriot. "A mechanical perspective on phagocytic cup formation". In: *Current Opinion in Cell Biology* 66 (Oct. 2020), pp. 112–122. ISSN: 0955-0674. DOI: 10.1016/J.CEB.2020.05.011.

[39] Benjamin Winkler et al. "Physical phase field model for phagocytosis". In: *New Journal of Physics* 26 (1 Jan. 2024), p. 013029. ISSN: 1367-2630. DOI: 10.1088/1367-2630/AD1A2E. URL: https://iopscience.iop.org/article/10.1088/1367-2630/ad1a2e%20https://iopscience.iop.org/article/10.1088/1367-2630/ad1a2e/meta.

[40] Sulin Zhang, Huajian Gao, and Gang Bao. "Physical Principles of Nanoparticle Cellular Endocytosis". In: *ACS Nano* 9.9 (2015). PMID: 26256227, pp. 8655–8671. DOI: 10.1021/acsnano.5b03184. eprint: https://doi.org/10.1021/acsnano.5b03184. URL: https://doi.org/10.1021/acsnano.5b03184.

[41] Jeroen S. Van Zon et al. "A mechanical bottleneck explains the variation in cup growth during FcγR phagocytosis". In: *Molecular Systems Biology* 5 (Jan. 2009), p. 298. ISSN: 17444292. DOI: 10.1038/MSB.2009.59. URL: /pmc/articles/PMC2736656/%20/pmc/articles/PMC2736656/?report=abstract%20https://www.ncbi.nlm.nih.gov/pmc/articles/PMC2736656/.